ANALYSIS AND DESIGN OF MICROSTRIP PATCH ANTENNAS WITH ARBITRARY SLOT SHAPES

A THESIS SUBMITTED TO
THE GRADUATE SCHOOL OF NATURAL AND APPLIED SCIENCES
OF
MIDDLE EAST TECHNICAL UNIVERSITY

BY

GÖKER ŞENER

IN PARTIAL FULFILLMENT OF THE REQUIREMENTS
FOR
THE DEGREE OF DOCTOR OF PHILOSOPHY
IN
ELECTRICAL AND ELECTRONICS ENGINEERING

APRIL 2011

Approval of the thesis:

ANALYSIS AND DESIGN OF MICROSTRIP PATCH ANTENNAS WITH ARBITRARY SLOT SHAPES

submitted by **GÖKER ŞENER** in partial fulfillment of the requirements for the degree of **Doctor of Philosophy in Electrical and Electronics Engineering Department, Middle East Technical University** by,

Prof. Dr. Canan Özgen _____
Dean, Graduate School of **Natural and Applied Sciences**

Prof. Dr. İsmet Erkmen _____
Head of Department, **Electrical and Electronics Engineering**

Assoc. Prof. Dr. Lale Alatan _____
Supervisor, **Electrical and Electronics Engineering Dept., METU**

Prof. Dr. Mustafa Kuzuoğlu _____
Co-supervisor, **Electrical and Electronics Engineering Dept., METU**

Examining Committee Members:

Prof. Dr. Seyit Sencer Koç
Electrical and Electronics Engineering, METU _____

Assoc. Prof. Dr. Lale Alatan
Electrical and Electronics Engineering, METU _____

Prof. Dr. Gülbin Dural
Electrical and Electronics Engineering, METU _____

Prof. Dr. Özlem Çivi
Electrical and Electronics Engineering, METU _____

Assoc. Prof. Dr. Yusuf Ziya Umul
Electronics and Communication Engineering, CANKAYA UNV. _____

Date: _____

I hereby declare that all information in this document has been obtained and presented in accordance with academic rules and ethical conduct. I also declare that, as required by these rules and conduct, I have fully cited and referenced all material and results that are not original to this work.

Name, Last Name: GÖKER ŞENER

Signature :

ABSTRACT

ANALYSIS AND DESIGN OF MICROSTRIP PATCH ANTENNAS WITH ARBITRARY SLOT SHAPES

Şener, Göker

Ph.D., Department of Electrical and Electronics Engineering

Supervisor : Assoc. Prof. Dr. Lale Alatan

Co-Supervisor : Prof. Dr. Mustafa Kuzuoğlu

April 2011, 70 pages

A new method is proposed that provides simple and efficient design and analysis algorithm for microstrip antennas with arbitrary patch shapes. The proposed procedure uses the muti-port network model (MNM) where the antenna is considered as a cavity bounded by perfect electric conductors on the top and the bottom surfaces and perfect magnetic conductor on the side surfaces. Ports are defined along the periphery of the patch, and the impedance matrix representing the voltage induced at one port due to a current source at another port, is obtained through the use of the 2-D Green's function corresponding to the cavity. For the MNM analysis of patches with irregular shapes such as slotted structures, the segmentation/desegmentation methods are utilized since the Green's function expressions are available only for regularly shaped cavities. To speed up the analysis and to develop a design procedure, vector Padé approximation is used in order to approximate the antenna impedance matrix as a rational function of two polynomials. When the approximation is performed with respect to frequency, the roots of the polynomial at the denominator provides the resonant frequencies of the antenna. The design algorithm is applicable when the approximation variable is changed to one of the dimensions of the patch that need to be optimized. Because for this case, the

roots of the denominator polynomial correspond to optimum dimensions of the antenna where it resonates.

Keywords: Slotted Antenna Analysis, Multiport Network Model, Irregularly Shaped Microstrip Antenna Analysis

ÖZ

DÜZENSİZ ŞEKİLLERDEKİ YARIKLI MİKROŞERİT ANTENLERİN ANALİZ VE TASARIMI

Şener, Göker
Doktora, Elektrik ve Elektronik Mühendisliği Bölümü
Tez Yöneticisi : Doç. Dr. Lale Alatan
Ortak Tez Yöneticisi : Prof. Dr. Mustafa Kuzuoğlu

Nisan 2011, 70 sayfa

Düzensiz yapıdaki mikrostrip yamalı antenlerin tasarım ve analizinde basit ve verimli yeni bir metod önerilmiştir. Önerilen bu yöntem çok kapılı ağ modeli kullanarak anteni bir kovuk olarak düşünüp üst ve alt yüzeyleri mükemmel elektrik iletken, yan yüzeleride mükemmel magnetik iletken olarak modellemektedir. Yama kenarları belirli sayıda portlara bölünerek bir porttaki akımdan endükte olan ve diğer porttaki voltajı belirten empedans matrisi, kovuk yapı için tanımlanan 2-D Green's fonksiyonun çözümünden bulunur. Düzgün olmaya yapıdaki yamalı antenlerde, örneğin yarıklı antenler gibi, birleştirme/ayrıştırma yöntemleri kullanılır zira Green's fonksiyonu sadece düzgün yapılarda bulunabilir. Tasarım ve analizi hızlandırmak için vektör Padé yakınsaması kullanılarak empedans matrisi polinomların rasyonel fonksiyonu şeklinde yakınsanmıştır. Yakınsama frekans ekseninde yapıldığı zaman paydadaki polinomun kökleri antenin resonant frekanslarına karşılık gelir. Antenin yama boyutlarını tasarlamak içinse yakınsama değişkeni optimize olacak boyutlardan biri olarak değiştirilir. Böylece polinomun kökleri resonant frekansındaki en uygun boyutları verir.

Anahtar Kelimeler: Yarıklı Anten Analizi, Çok Kapılı Ağ Yöntemi, Değişken Yapıda Mikrostrip Anten Analizi

To My Son, Erdem Kıvanç Şener

ACKNOWLEDGMENTS

I would like to thank to my advisors, Prof. Dr. Mustafa Kuzuoğlu and Assoc. Prof. Dr. Lale Alatan for all their guidance and support throughout the work of this project. Their insights, wealth of knowledge, and helpful personalities have been an inspiration and a guidance through this thesis.

In addition, I would like to extend sincere appreciation to Prof. Dr. Seyit Sencer Koç and Assoc. Prof. Dr. Yusuf Ziya Umul for their guidance and support.

I also thank to all the instructors in the Middle East Technical University Electrical Engineering department for their assistances and teaching efforts.

To my wife, Ebru Şener, I offer sincere thanks for her dedication and motivation at all times.

To my mother and father, I thank them for their understanding and self-sacrifices throughout my life.

Vita: Göker Şener was born at Balıkesir, Turkey, on April 21, 1973. He received the B.E. in electrical engineering in 1995 from the Wright State University, OH./USA., and M.E. degree in electrical engineering in 2004 from the Middle East Technical University Ankara/Turkey. He worked with the company ”ASELSAN” during 1995-1996, and completed his military service in 1997. Since 1999, he has been working as an instructor in Çankaya University electrical and electronics engineering department. His fields of interest are antenna theory, microstrip antennas and numerical techniques.

TABLE OF CONTENTS

LIST OF TABLES

TABLES

LIST OF FIGURES

FIGURES

CHAPTER 1

INTRODUCTION

A microstrip antenna, in its simplest form consists of a radiating patch on one side of the dielectric substrate and a ground plane on the other side, Fig.1.1. A microstrip antenna could be excited in various ways that could be classified into two groups; direct feeding and coupled feeding. Coaxial line feed and microstrip line feed are examples to direct feeding. Aperture coupled feed and electromagnetically coupled feed are examples to coupled feeding techniques.

The appropriate feeding technique is generally chosen according to the specifications of the antenna and the requirements of the application. Microstrip antennas are preferred in a wide range of applications such as aircraft antennas, missile guidance antennas, mobile radios and array antennas due to their advantageous features as being low profile, having low fabrication costs and ease of integration with microwave circuits. However, microstrip antennas also have some disadvantageous characteristics like having narrow bandwidth and low power handling

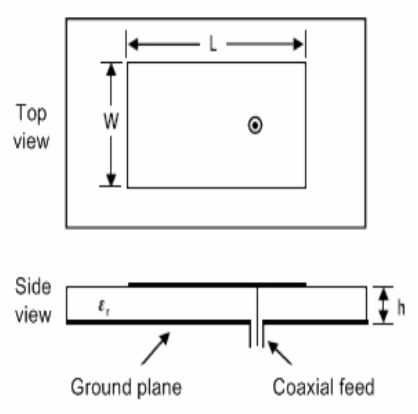

Figure 1.1: Microstrip antenna [22]

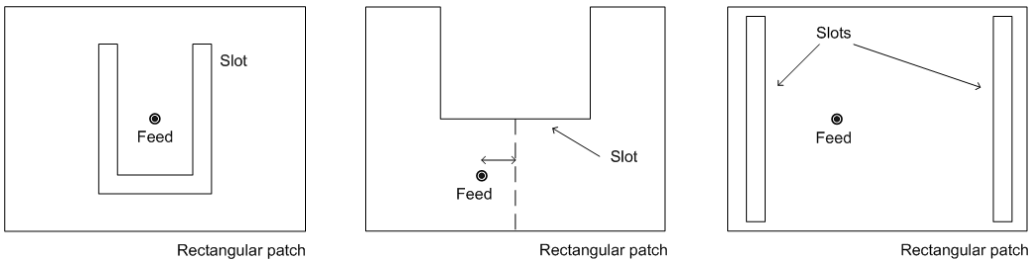

(a) u-slotted antenna (b) cmsa (c) dual-band antenna

Figure 1.2: Some irregularly shaped microstrip antennas

capacity. Therefore, there has been a vast amount of research on proposing alternative microstrip antenna configurations that could eliminate the drawbacks of conventional microstrip antennas. As alternative antenna configurations, introduction of parasitic patches (either on the same substrate with the excited patch or on other substrates of a multilayer structures) and modifying the shape of the microstrip patch are proposed. Since the focus of this thesis is on the analysis and design of microstrip antennas with arbitrary slot shapes, a brief review of some alternative antenna structures that rely on the modification of the patch shape will be presented.

To increase the bandwidth, it is required that two or more resonant frequencies are closely spaced. For this purpose, a rectangular patch with a u-shaped slot as shown in Fig.1.2(a) has been proposed in [1], where it is reported that by introducing the slot, 47% is achieved for a microstip antenna with 0.08 wavelength thick air substrate. It is also noted that the bandwidth drops to 12.4% when the substrate height is decreased to 0.04 wavelength but the bandwidth is still considerably larger than for the patch without the u-slot.

For antenna array applications and some mobile applications, miniaturization of the antenna is required. The resonance frequency of the patch antenna is inversely proportional to the length of the antenna. Therefore, the dimensions of the antenna could be reduced by increasing the effective length of the patch. To achieve this, the geometry shown in Fig.1.2(b) is proposed in [2]. In this configuration, the effective length is increased by the slot due to the increase in the surface current path length. Hence, the antenna resonates at a lower frequency than a rectangular microstip antenna of the same size.

Dual frequency operation is required in mobile communication systems where two differ-

ent communication bands such as GSM (Global System for Mobile Communication, 880-960MHz), DCS (Digital Cellular System, 1710-1880 MHz), PCS (Personal Communication Service, 1850-1990 MHz), UMTS (Universal Mobile Telecommunication System, 1920-2170 MHz), are combined in one system. To obtain dual frequency operation with a microstrip antenna, the structure shown in Fig.1.2(c) has been proposed in [3]. As will be discussed later in this chapter, microstrip antennas could support TM_{n0} modes. Among these, TM_{10} and TM_{30} could be used for dual frequency operation (TM_{20} is not used since it exhibits a null field at the broadside direction). The frequency ratio of these modes are approximately 3. Slots lower this ratio by modifying the fields distribution of the TM_{30} mode.

Throughout this thesis, the microstrip antenna with the patch cut in different shapes in order to fulfill a specific antenna property such as compactness, wideband characteristics or multi-resonant operation will be referred as irregularly shaped patch antenna.

Although successful design examples of irregularly shaped patch antennas antennas with slots could be found in literature, to the author's knowledge, no procedure or guidelines for the design of similar antennas have been reported. Hence, the main aim of this thesis work is to develop a method that provides simple and efficient design algorithm. Among the various analysis methods that are used to analyze microstrip antennas, multiport network model is chosen in this work. In order to justify this choice, analysis methods will be summarized. These methods are divided into two groups: analytical and numerical techniques. Generally accepted analytical methods are the transmission line model, cavity model and multiport network model. Numerical methods are the finite difference time domain (FDTD) method, finite element method (FEM) and method of moments (MoM).

In the transmission line model, the rectangular patch is modeled as a part of a transmission line as shown in Fig.1.3(a). The two open ends of the patch where the radiation takes place are represented by admittances. The characteristic impedance, propagation constant and edge admittance values of the transmission line can be found through the use of some empirical formulas [22]. The real part of this admittance is associated with the power radiated from the edge, and the imaginary part represents the energy stored in the fringing fields close to the edge. Although the transmission line model is easy to use, it only considers the dominant mode of the antenna, so higher order modes can not be analyzed by using this model. Moreover, the method is not applicable to microstrip antennas with slots.

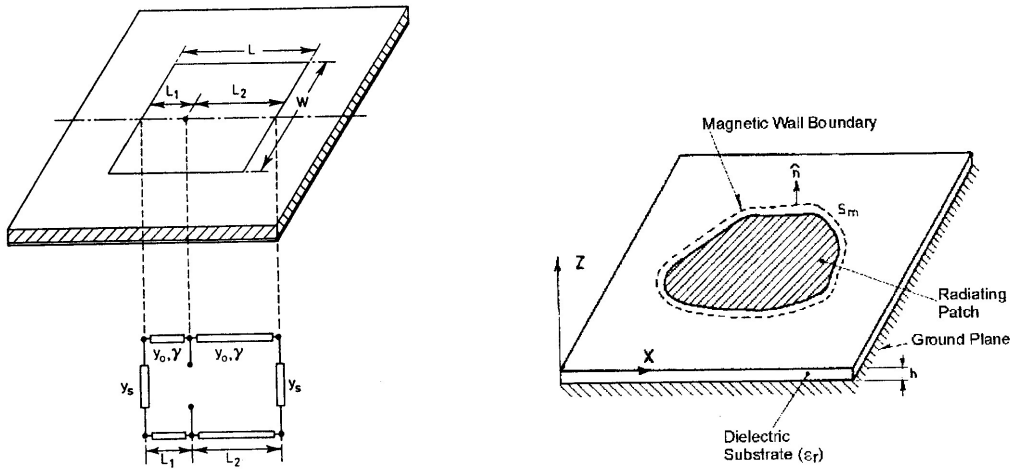

(a) Transmission line model

(b) Cavity model

Figure 1.3: Methods of analysis [32]

In the cavity model, the thickness of the substrate is restricted to be small compared to a wavelength, so that the fields under the patch can be assumed to be constant. As a result of this assumption, the electric field has only z component, while the magnetic field has only x and y components in the region bounded by the microstrip patch and the ground plane. In addition, since the electric current in the microstrip must not have a component normal to the edge, it follows from Maxwell's equations that the tangential component of magnetic field along the edge should also be zero. Hence, the region between the patch and the ground plane can be considered as a cavity bounded by electric walls on the top and bottom, and by a magnetic wall on the side, Fig.1.3(b). Field solutions for the cavity subjected to these boundary conditions can be easily obtained from the solution of Maxwell's equations.

Multiport network model (MNM) is an extension to cavity model. The effect of fringing fields at the edges of the antenna is ignored in the cavity model since the side walls of the dielectric resonator is assumed to be perfect magnetic conductors. To incorporate the effect of fringing fields into the cavity model, discrete number of ports is placed along the periphery of the patch and these ports are terminated by edge admittances that account for the radiated power and the stored energy of the antenna. Consequently, the patch is modeled as a "multiport network" and the port voltages and currents are related to each other through an impedance matrix. The entries of the impedance matrix involve the electric field Green's function of the dielectric resonator due to a vertical electrical dipole, which is analytically

available for rectangular, circular and triangular shaped resonators. MNM is first introduced in 1972 [4],[5], about a decade later the use of MNM in conjunction with segmentation [6] and desegmentation [7] methods are proposed to analyze two dimensional microwave circuits. In segmentation method, the arbitrarily shaped printed structure is decomposed into rectangular sections, the impedance matrix of each section is calculated and then they are combined through the use of connectivity information of the ports to obtain the impedance matrix of the whole structure. The use of segmentation and/or desegmentation method made it possible to analyze microwave printed circuits other than microstrip antennas. As representative examples, a two-port unequal power divider [8] and a multistage wideband power divider [9] can be listed. Moreover, the application of MNM and segmentation/desegmentation methods for the analysis of several irregularly shaped patch antennas can be found in [10],[11] for circularly polarized microstrip antennas, in [2] for compact antennas, in [12] for dual-band antennas and in [13],[14] for directly coupled broadband antennas.

The original MNM was proposed for the analysis of microstrip antennas fed by coaxial probes. Later the method is extended to include the analysis of other feeding structures such as electromagneticly coupled [15] and aperture coupled [16], [17] configurations. In addition, a two-port microstrip antenna is studied in [18] and a superstrate dielectric layer on top of the patch is consider in [19]. The method is further improved to analyze stacked microstrip antennas [20]. The analysis of mutual coupling effects in microstrip antenna arrays via the MNM became possible through the use of coupling networks proposed in [21].The details of the multiport network model will be presented in Chapter 2.

In order to analyze the structure via numerical methods, first the structure is discretized then the integral and/or differential equations are transformed into matrix equations. In the FDTD method, spatial as well as time grid for the electric and magnetic fields are generated. Each cell contains information about material characteristics. A matrix equation is obtained by approximating the partial derivatives in Maxwell's curl equations with finite difference formulas. The cells containing the sources are excited with a suitable excitation function, which propagates along the structure. The discretized time variations of the fields are determined at desired locations. The input impedance of the antenna is obtained by computing the voltage at the excitation port via a line integral of the electric field and by computing the current at the port through a loop integral of the magnetic field. The Fourier transform of the time domain solution yields the frequency response of the structure.

In the FEM, the region of interest is divided into surface and/or volume elements depending on the geometry of the structure to be analyzed. These discretized units, generally referred to as finite elements, can be any well-defined geometrical shapes such as triangular elements for planar configurations and tetrahedral and prismatic elements for three-dimensional configurations, which are suitable even for curved geometries.

In FDTD and FEM, the whole solution space is dicretized. Since microstrip antenna is an open radiating structure, the solution space need to be truncated in order to be able to apply FDTD and FEM. Perfectly Matched Layers (PML) proposed in [23] provides a very accurate truncation scheme.

In the MoM, the surface currents are used to model the microstrip patch. An integral equation is formulated for the unknown currents on the microstrip patches and the feed lines. The unknown currents are expanded in terms of known basis functions. Then the boundary condition on the conducting patch is enforced by taking the inner product integral of the integral equation with a set of testing functions. Consequently, the integral equation is transformed into a matrix equation, where the matrix entries involve the Green's function for the grounded dielectric slab. However, the Green's function of the grounded dielectric slab is necessary to evaluate the matrix entries. In order to obtain the Green's function in space domain, the evaluation of the Sommerfeld integral is necessary. This integral is highly oscillatory and slowly convergent. Hence, methods such as discrete complex image method (DCIM) [24] have been proposed for the efficient computation of the spatial domain Green's function. In the MoM, only surface currents are unknown, hence there is less number of unknowns compared to FEM and FDTD methods.

In the design of microstrip patch antennas, the FDTD and FEM offer trial and error search techniques. Only MoM provides a guided search algorithm, however in MoM, meshing should be very fine for the optimization of the slotted patch structures. Therefore, the number of unknowns increases, and makes the method inapplicable for a directed search.

When the optimization of the antenna dimensions through the use of numerical methods is considered, either the matrix equation corresponding to different dimensions should be constructed and solved for each iteration of the optimization algorithm or the antenna should be discretized with very fine meshes in order to make a discrete search for the optimum solution. Both of these approaches are computationally inefficient since the former approach requires

the construction and the solution of the matrix equation at each iteration and the later one results in a matrix equation of very large size. Consequenctly when the use of numerical techniques in the design of microstrip antennas is considered, optimization of the patch shape instead of optimization of the antenna dimensions is preferred. Because to optimize the shape of the patch, the whole matrix corresponding to a rectangular patch could be first constructed and the matrix corresponding to a irregularly shaped patch can be formed by selecting the appropriate rows and columns from the original matrix. Since this type of an approach is very suitable to be used in conjunction with genetic algorithms (GA), where the optimization parameters are binary encoded, microstrip antenna design examples with the use of MoM and GA are proposed in [25].

The utilization of MNM in the optimization of the antenna dimensions also requires the construction and the solution of the impedance matrix at each iteration of the optimization algorithm. However, this approach is more feasible compared to the use of MoM, since only the periphery of the patch is discretized in MNM and consequently the number of unknowns are much less than that of MoM where whole patch surface is dicretized. For this reason, multiport network model is chosen as the analysis method in this thesis. To speed up the analysis within a frequency band, Padé approximation [26] is used. The Padé approximation of a function is the ratio of two polynomials. The coefficients of the polynomials are obtained by equating the approximated function to its Taylor series expansion. There are some examples of the application of Padé approximation to electromagnetic problems such as the analysis of cavity-backed microstrip antennas by FEM [33]. However, in all these applications, scalar Padé has been used, that is the Padé approximation of each matrix entry is obtained individually. The poles of each matrix entry are the zeros of the polynomial at the denominator of the Padé approximation. When the matrix equation is considered as the transfer function of the system, it is expected that denominator polynomials should be same for the whole matrix. This expectation is also verified by numerical examples. Based on this result, the use of vector Padé approximation [26] is proposed. When a vector of functions is considered, vector Padé method provides a rational function approximation with a common denominator polynomial and a vector of numerator polynomials. This work will be the first application of the vector Padé approximation in the field of electromagnetics.

Poles of the approximation are the singularities that correspond to resonance modes of the antenna. When the dimensions of the antenna are given and the Padé approximation is obtained

with respect to frequency, the zeros of the denominator polynomial provide the resonance frequencies of the antenna. Similarly when the frequency is fixed and the Padé approximation is obtained with respect to one of the dimension of the antenna, the zeros of the denominator polynomial provide the optimum length for which the resonance occurs. Thus, through the use of an algorithm based on the Padé approximation with respect to the dimensions of the antenna, it is possible to find optimum antenna dimensions without the necessity of any optimization algorithm.

Chapter 2 introduces the multiport network model. Formulation of the impedance matrix for a rectangular patch antenna is presented followed by the segmentation and the desegmentation methods that enable the analysis of irregularly shaped patch antennas. The MNM analyses of some microstrip antenna structures with slots are performed and their results are presented. The numerical results are compared to the results obtained from the electromagnetic simulation software IE3D by Zeland software, to demonstrate the accuracy of the MNM.

Chapter 3 presents the formulation of the Padé and the vector Padé approximations. The implementation of the vector Padé approximation to a demonstrative example is included to assist the explanation of the rather complicated steps of the approximation procedure.

Chapter 4 is devoted to the application of the vector Padé approximation to the MNM. First, the Padé approximation is performed with respect to frequency, and the frequency response of the example structures studied in Chapter 2 are obtained for different orders of approximating polynomial with different expansion points. The accuracy of the approximation with respect to the order of the approximating polynomial and the expansion point is discussed and the improvement in the computation time via the use of Padé approximation is presented. Then, the design of irregularly shaped patch antennas through the use of the Padé approximation with respect to the dimensions of the antenna is presented together with some design examples.

Finally, conclusions of the thesis and the future work are presented in Chapter 5.

CHAPTER 2

MULTIPORT NETWORK MODEL

In this chapter, the Multiport Network Model (MNM) which is an analytical method developed to analyze printed microwave circuits such as microstrip antennas, will be presented. A typical microstrip antenna configuration is shown in Fig.2.1 to define the parameters, unit vectors and the coordinate axis adopted throughout this thesis.

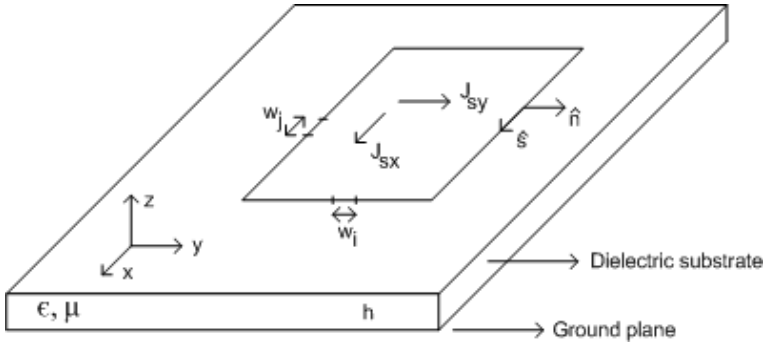

Figure 2.1: Geometry of the problem

The formulation of the method starts with the assumption that the thickness of the dielectric substrate is small compared to the wavelength so that the field variations in the substrate can be assumed to be zero along z direction($\partial/\partial z = 0$). When this assumption is combined with the boundary conditions on the conducting patch, two important results that form the basis of the MNM can be obtained. First of all, the normal component of the surface currents ($\hat{n} \cdot \bar{J}_s$) flowing on the patch should be zero at the edges. Consequently, the tangential component of the magnetic field ($\hat{s} \cdot \bar{H}$) is zero at the edges of the patch. Since no field variation is assumed in z direction, the tangential component of the magnetic field should be zero starting from the edge of the patch extending down to the ground plane. Therefore, the patch antenna

can be modeled by a rectangular dielectric resonator bounded by perfect electric conductors (PEC) on the top and the bottom surfaces and by perfect magnetic conductors (PMC) on the side walls. Also, the tangential electric field components vanish on the patch surface and the ground plane. Since the field is assumed to be constant along z direction, the transverse electric field components E_x and E_y should be zero under the patch. From Maxwell's equations, this also implies that $H_z = 0$. Thus, the structure supports only TM^z waves. The only nonzero field components that are related by Maxwell's equations are given as

$$j\omega\epsilon E_z = \frac{\partial H_y}{\partial x} - \frac{\partial H_x}{\partial y} \tag{2.1}$$

$$-j\omega\mu H_x = \frac{\partial E_z}{\partial y} \tag{2.2}$$

$$j\omega\mu H_y = \frac{\partial E_z}{\partial x} \tag{2.3}$$

where ω is the radian frequency, ϵ is the substrate permittivity and μ is the substrate permeability. By substituting (2.2) and (2.3) into (2.1), the following equation is obtained for E_z.

$$(\nabla_t^2 + k^2)E_z = 0 \tag{2.4}$$

where ∇_t^2 is the transverse Laplacian operator and $k = \omega\sqrt{\mu\epsilon}$ is the wavenumber in the dielectric substrate. Since the only field component is the vertical E_z, the voltages around the periphery can be defined as $V = hE_z$. To model the field variations in the transverse directions, the periphery of the patch is divided into small sections called "ports". The widths of the ports (w_j) are chosen such that the circuit variables (voltage and current) can be assumed to remain constant throughout the extend of the port. This assumption leads to define the port voltage ($\bar{V}_j$) and the port current ($\bar{I}_j$) at the j^{th} port as

$$\bar{V}_j \equiv \frac{h}{w_j}\int_{w_j} E_z(s_j)ds_j \quad , \quad \bar{I}_j \equiv w_j J_{zj} \tag{2.5}$$

where J_{zj} is the z-directed surface current density at port j. The integral is taken with distance variable "s_j" along the width of the j^{th} port. It can be easily shown that when a z-directed current density is considered, the homogeneous Helmholtz equation obtained in (2.4) becomes an inhomogeneous Helmholtz equation given as

$$(\nabla_t^2 + k^2)E_z = j\omega\mu J_z \tag{2.6}$$

Solution of this differential equation at the observation point (x, y) can be expressed in terms of the Green's function, $G(x, y|x_0, y_0)$, corresponding to the rectangular dielectric resonator

due to a vertical electrical dipole at (x_0, y_0) as:

$$E_z(x,y) = \int\int G(x,y|x_0,y_0)J_z(x_0,y_0)dx_0dy_0 \tag{2.7}$$

By combining equations (2.5) and (2.7), the port voltage of the i^{th} port can be written in terms of the port current at the j^{th} port as:

$$\bar{V}_i = \frac{h}{w_i}\int\int G(x_i,y_i|x_j,y_j)\frac{\bar{I}_j}{w_j}ds_jds_i \tag{2.8}$$

If there are N ports along the periphery of the patch, then an impedance matrix (Z) of $N \times N$ can be defined relating port voltages to port currents. The entries of this impedance matrix can be written as:

$$\tilde{Z}^E_{ij} = \left.\frac{\bar{V}_i}{\bar{I}_j}\right|_{\bar{I}_i=0, i\neq j} = \frac{h}{w_iw_j}\int_{w_i}\int_{w_j} G(x_i,y_i|x_j,y_j)ds_ids_j \tag{2.9}$$

$\bar{I}_i = 0, i \neq j$ refers that all ports except for the j^{th} port are open circuited. The eigenfunction representation of the electric field Green's function for a rectangular dielectric resonator of size ($W \times L$) surrounded by PMC can be written as [23]:

$$G(x,y|x_0,y_0) = j\omega\mu\sum_{m=0}^{\infty}\sum_{n=0}^{\infty}\frac{\sigma_m\sigma_n\cos(k_xx)\cos(k_yy)\cos(k_xx_0)\cos(k_yy_0)}{k_x^2+k_y^2-k^2} \tag{2.10}$$

where

$$\begin{aligned} k_x &= m\pi/L \;\; and \;\; k_y = n\pi/W \\ \sigma_m &= 1, \;\; if \;\; m = 0 \;\; and \\ \sigma_m &= 2, \;\; otherwise \\ k^2 &= \omega^2\mu_0\epsilon_0\epsilon_e(1-j\delta_e) \end{aligned} \tag{2.11}$$

where ϵ_e is the effective dielectric constant and δ_e is the loss tangent of the substrate.

Substituting (2.10) in (2.9) and evaluating the integral yields

$$Z_{ij} = \frac{j\omega\mu\ h}{w_iw_j}\sum_{m=0}^{\infty}\sum_{n=0}^{\infty}\frac{\sigma_m\sigma_n\cos(k_xx_i)\cos(k_yy_i)\cos(k_xx_j)\cos(k_yy_j)}{k_x^2+k_y^2-k^2}\text{sinc}(k_xw_i/2)\text{sinc}(k_yw_j/2) \tag{2.12}$$

where (x_i, y_i) denotes the coordinates of the center point of the i^{th} port.It should be noted that the spectral wave numbers k_x and k_y that appear in the argument of sinc functions refer to the orientation of the ports. Therefore, (2.12) corresponds to a matrix entry where i^{th} port is along x-direction and j^{th} port is along y-direction.

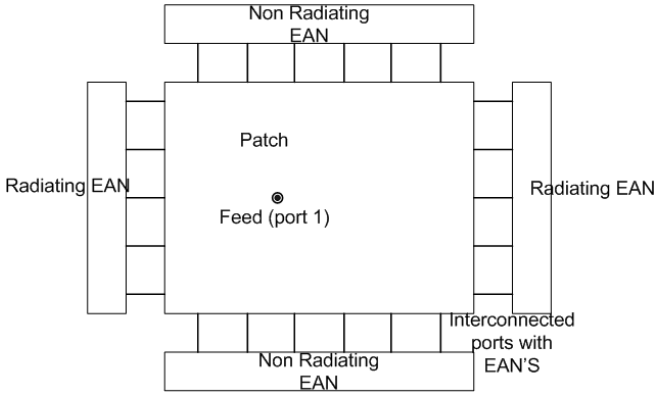

Figure 2.2: Multiport network model of a rectangular patch antenna incorporating EAN's

After constructing the impedance matrix, each port is terminated by an edge admittance that accounts for the fringing fields at the edges and the radiated power from the antenna. Two types of edge admittance networks (EAN) are defined as shown in Fig.2.2. Radiating edge admittance networks are connected to the radiating edges of the antenna and they include both real and imaginary parts that represent the radiated power and the energy stored in the fringing fields at the edges. On the other hand, non-radiating edge admittance networks involve only imaginary parts to represent the effect of fringing fields.

For incorporating edge admittance networks in the multiport network model for microstrip patch antennas, a capacitance-conductance pair (B,G) is connected to each port of the equivalent multiport model of the patch [23]. The conductance G contains two parts: a radiation conductance G_r, and a surface-wave conductance G_s. Radiation conductance is the ohmic conductance that corresponds to equivalent radiated power from the edge. If the edge has width W and the power radiated from the edge for a uniform voltage distribution is P_{rad}, the radiation conductance per unit length of the edge is given by $2P_{rad}/W$, where P_{rad} is calculated for a unit voltage at the edge. If continuous voltage distribution $V(s)$ is considered along the edge with s being the length parameter, then the radiation conductance per unit length is obtained as

$$\frac{G_r}{W} = \frac{2P_{rad}}{\int_0^W V^2(s)ds} \tag{2.13}$$

Similarly, if P_s is the power coupled to the surface waves, the surface wave conductance per

unit length is given as

$$\frac{G_s}{W} = \frac{2P_s}{\int_0^W V^2(s)ds} \tag{2.14}$$

For n uniformly spaced ports, the conductance per port can be obtained by G_r/n and G_s/n for radiation and surface wave conductances, respectively. Hence, a uniform conductance distribution is assumed. Similar to edge conductance, the edge susceptance is also considered to be uniformly distributed along the edge.

Capacitance and conductance values that need to be connected to an edge can be obtained by various formulations reported in the literature. Here, the most common formulations will be presented.

2.1 Edge Conductance

The most widely used formula for the edge conductance has been given by James [23]. It is obtained by modeling the two radiating edges by two slots that radiate in upper half space. For an edge with width (W), the associated edge conductance is as follows:

$$G_r = \begin{cases} \frac{W_e^2}{90\lambda_0^2} & (W_e \leq 0.35\lambda_0) \\ \frac{W_e^2}{120\lambda_0} - \frac{1}{60\pi^2} & (0.35\lambda_0 \leq W_e \leq 2\lambda_0) \\ \frac{W_e}{120\lambda_0} & (2\lambda_0 < W_e) \end{cases} \tag{2.15}$$

where λ_0 is the free space wavelength, and W_e is the effective width of the resonator of width W. The effective width can be obtained as follows:

$$W_e = 2\pi h / ln\left[hF/W' + \sqrt{1 + (2h/W')^2}\right] \tag{2.16}$$

$$F = 6 + (2\pi - 6)exp[(-4\pi^2/3)(h/W')^{3/4}] \tag{2.17}$$

$$W' = W + (t/\pi)\left[1 + ln\left\{4/\sqrt{(t/h)^2 + (1/\pi)^2/(W/t + 1.1)^2}\right\}\right] \tag{2.18}$$

where t is the thickness of the patch conductor.

A more precise formula for the edge conductance has been given by Van De Capelle [23] as follows:

$$\begin{aligned} G_r =& \frac{1}{\pi\eta_0}\left\{\left[k_0 W_e si(k_0 W_e) + cos(k_0 W_e) + \frac{sin(k_0 W_e)}{k_0 W_e} - 2\right]\right. \\ &\left.\times\left(1 - \frac{(k_0 h)^2}{24}\right) + \frac{(k_0 h)^2}{12}\left[\frac{1}{3} + \frac{cos(k_0 W_e)}{(k_0 W_e)^2} - \frac{sin(k_0 W_e)}{(k_0 W_e)^3}\right]\right\} \end{aligned} \tag{2.19}$$

where $\eta_0 = 120\pi$ is the free space wave impedance, k_0 is the free space wave number, and h is the substrate height. The function $si(x)$ is defined as

$$si(x) = \int_0^x \frac{sin(u)}{u} du \tag{2.20}$$

2.2 Edge Susceptance

As in the case of edge conductance, several different formulations are available for edge susceptance also. One of the formulas is based on the capacitance of open-end microstrip lines, and given by [23]

$$B = 0.01668 \frac{\Delta a}{h} \frac{W_e}{\lambda_0} \epsilon_r \tag{2.21}$$

where

$$\frac{\Delta a}{h} = 0.412 \frac{(\epsilon_r + 0.3)(W/h + 0.264)}{(\epsilon_r - 0.258)(W/h + 0.8)} \tag{2.22}$$

Another formulation for $\frac{\Delta a}{h}$ is given as

$$\frac{\Delta a}{h} = \frac{0.95}{1 + 0.85 k_0 h} - \frac{0.075(\epsilon_r - 2.45)}{1 + 10 k_0 h} \tag{2.23}$$

In another approach [23] that is developed to include the effects of fringing fields, the dimensions of the antenna are increased, the edge susceptances are omitted and the edge admittances are expressed only in terms of edge conductance values. The extension ΔL in the length of the patch dimension to account for the fringing fields is given by [22]

$$\Delta L = h \xi_1 \xi_3 \xi_5 / \xi_4 \tag{2.24}$$

where

$$\xi_1 = 0.434907 \frac{\epsilon_e^{0.81} + 0.26}{\epsilon_e^{0.81} + 0.189} \frac{(W/h)^{0.8544} + 0.236}{(W/h)^{0.8544} + 0.87} \tag{2.25}$$

$$\xi_2 = 1 + \frac{(W/h)^{0.371}}{2.358\epsilon_r + 1} \tag{2.26}$$

$$\xi_3 = 1 + \frac{0.5274 arctan[0.084(W/h)^{1.9413/\xi_2}]}{\epsilon_e^{0.9236}} \tag{2.27}$$

$$\xi_4 = 1 + 0.0377 arctan[0.067(W/h)^{1.456}]6 - 5exp[0.036(1 - \epsilon_r)] \tag{2.28}$$

$$\xi_5 = 1 - 0.218 exp(-7.5 W/h) \tag{2.29}$$

The extension in the patch dimensions reduces with an increase in frequency. This frequency dependent dispersion effect is accounted by replacing ϵ_e by $\epsilon_e(f)$ where ϵ_e is given by [22]

$$\epsilon_e = 0.5[\epsilon_r + 1 + (\epsilon_r - 1)G] \tag{2.30}$$

where

$$G = \left(1 + \frac{10h}{W}\right)^{AB} - \frac{ln4}{\pi}\frac{t}{\sqrt{Wh}} \tag{2.31}$$

$$A = 1 + \frac{1}{49}ln\left[\frac{(W/h)^4 + W/(52h)^2}{(W/h)^4 + 0.432}\right] + \frac{1}{18.7}ln\left[1 + \left(\frac{W}{18.1h}\right)^3\right] \tag{2.32}$$

$$B = 0.564exp[-0.2/(\epsilon_r + 0.3)] \tag{2.33}$$

The frequency dependent permittivity is given by

$$\epsilon_e(f) = \epsilon_r - (\epsilon_r - \epsilon_e)/(1 + P) \tag{2.34}$$

where

$$P = P_1P_2[(0.1844 + P_3P_4)f_n]^{1.5763} \tag{2.35}$$

$$P_1 = 0.27488 + [0.6315 + 0.525/(1 + 0.0157f_n)^{20}]u - 0.65683exp(-8.7513u) \tag{2.36}$$

$$P_2 = 0.33622[1 - exp(-0.03442\epsilon_r)] \tag{2.37}$$

$$P_3 = 0.0363exp(-4.6u)[1 - exp-(f_n/38.7)^{4.97}] \tag{2.38}$$

$$P_4 = 1 + 2.751[1 - exp-(\epsilon_r/15.916)^8] \tag{2.39}$$

$$f_n = f.h(in\ GHz.mm) = 47.713kh \tag{2.40}$$

$$u = [W + (W' - W)/\epsilon_r]/h \tag{2.41}$$

In the next section, some numerical examples are studied to investigate the accuracy levels of the EAN's presented above. The results are compared to the results obtained through a MoM based commercially available electromagnetic simulation software called IE3D by Zealand software.

2.3 Numerical examples

If the feed port is set to be the first port in the multiport network model, then Z_{11} gives the input impedance of the antenna. By equating the port current corresponding to the feed port to 1 and by equating the other port currents to zero, the port voltages can be calculated. Once the port voltage values are found, the radiation pattern of the antenna can be computed through the use of the formulation presented in Appendix A.

Before going to the details of the numerical results, some numerical issues that are critical during the implementation of MNM will be discussed.

In the evaluation of the Green's function, the summation over the eigenfunction modes should be truncated. According to Pang [10], this value should be greater than 4k where k is the wavenumber. In this thesis, the summation is truncated at 40 modes, since it is observed that this number yields accurate results when compared to IE3D.

The port width W_i is chosen typically about $\lambda/10$ for many applications while more ports should be taken if the field variation is rapid.

To assess the accuracy of the EAN formulations, a rectangular patch antenna with dimensions L=6cm, W=4cm build on a substrate of dielectric constant ϵ_r=2.33, is analyzed via MNM for three different substrate thicknesses. Two different cases of EAN formulations are used in the analysis: The edge admittance formulations given by (2.18) for G and (2.21) for B and the effective length formulation in (2.24). Simulation results for the input return loss obtained through MNM with these edge admittance formulations, through MNM withot modeling the edge effects and through IE3D are presented in Fig.2.3(a), Fig.2.3(b) and Fig.2.3(c) for substrate thicknesses, h=1.59 mm, h=5 mm and h=10 mm, respectively. With reference to the simulation results obtained from IE3D, it is found that using effective length formulation gives the most accurate results. In addition, as the substrate thickness increases, all methods begin to decrease in accuracy. Therefore, throughout this thesis, electrically thin dielectric substrates are studied with effective length formulation in multiport analysis.

As discussed in the introduction chapter, for the analysis of irregularly shaped microstrip patch antennas such as slotted antennas, the segmentation method or de-segmentation method need to be utilized in conjunction with multiport network model. Hence, the segmentation and the desegmentation methods will be presented in the following sections.

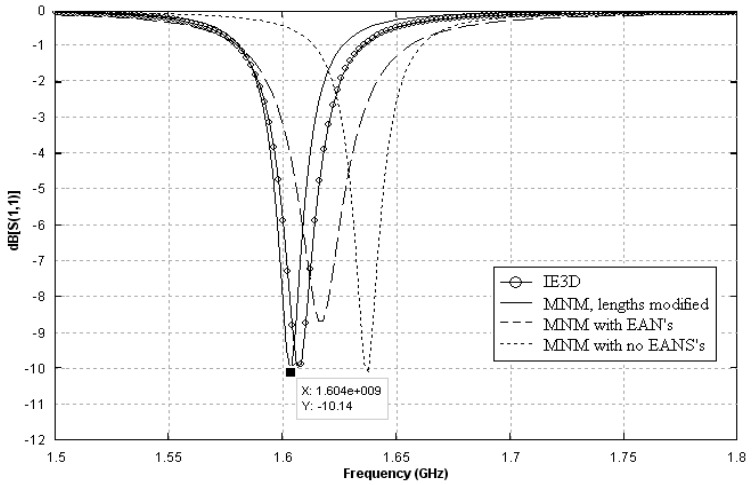

(a)

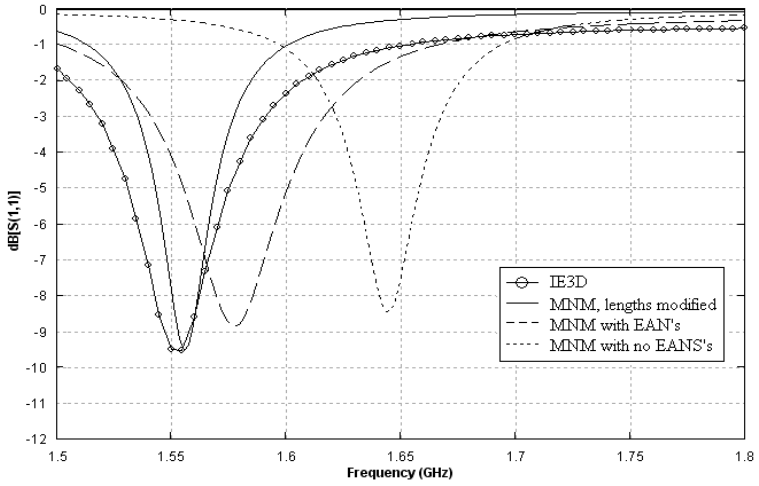

(b)

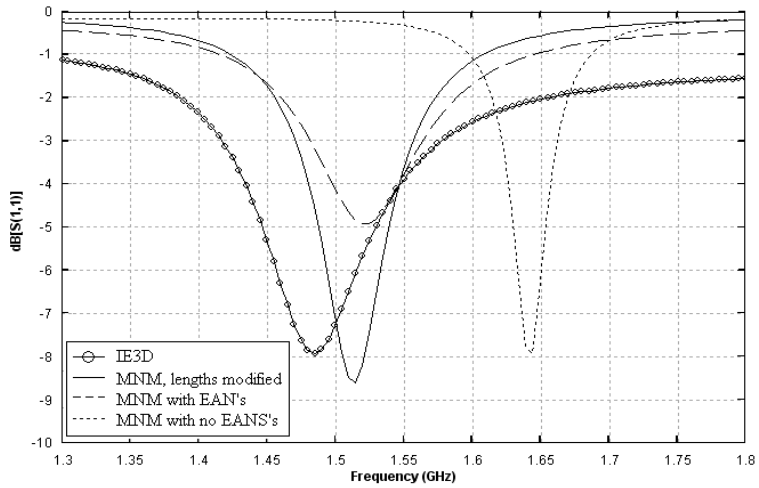

(c)

Figure 2.3: Effects of EAN formulation in the MNM anaysis of the RMSA with thickness (a) h=1.59mm, (b) h=5mm, (c) h=10mm

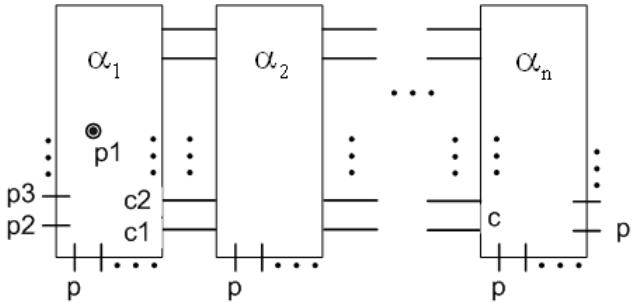

Figure 2.4: Segmentation of n-segments, $\alpha_1, ..., \alpha_n$, to form the overall shaped patch segment.

2.4 Segmentation Method

In the segmentation method, the arbitrarily shaped patch antenna is divided into rectangular segments as shown in Fig.2.4. In a general network of these n-segments, Z-matrices can be written together as

$$\begin{bmatrix} \bar{V}_p \\ \bar{V}_c \end{bmatrix} = \begin{bmatrix} \tilde{Z}_{pp} & \tilde{Z}_{pc} \\ \tilde{Z}_{cp} & \tilde{Z}_{cc} \end{bmatrix} \begin{bmatrix} \bar{I}_p \\ \bar{I}_c \end{bmatrix} \tag{2.42}$$

where $\bar{V}_p$, $\bar{I}_p$ and $\bar{V}_c$, $\bar{I}_c$ are the voltages and currents at the p external and c internal (connected) ports, respectively [6]. The voltages at the connected ports should be equal and the sum of the currents of the connected ports should be zero. Through the use of connectivity matrices Γ_1 and Γ_2 that define the topology, these two constraints can be expressed as:

$$\Gamma_1 \bar{V}_c = \bar{0} \tag{2.43}$$

$$\Gamma_2 \bar{I}_c = \bar{0} \tag{2.44}$$

In Γ_1 and Γ_2 matrices all entries in a row are zero except for the two entries in the columns corresponding to the connected ports. The two nonzero entries in a row are 1 and -1 for matrix Γ_1 and both 1 for matrix Γ_2.

Combining (2.42), (2.43) and (2.44), one can obtain the relation between I_p and I_c as,

$$\begin{bmatrix} \Gamma_1 \tilde{Z}_{cc} \\ j\Gamma_2 \end{bmatrix} \bar{I}_c = \begin{bmatrix} -\Gamma_1 \tilde{Z}_{cp} \\ \tilde{0} \end{bmatrix} \bar{I}_p \tag{2.45}$$

Substituting the value of I_c, obtained from (2.45) into (2.42), we get the overall network

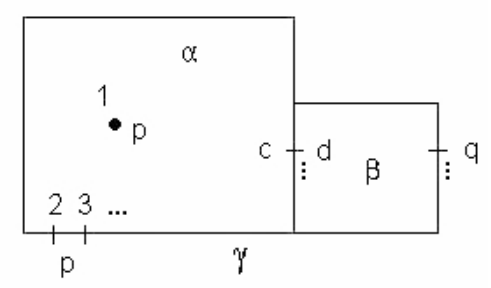

Figure 2.5: Segmentation of two rectangular segments α and β to form the irregularly shaped γ segment.

impedance matrix as

$$\tilde{Z}_p = \tilde{Z}_{pp} - \tilde{Z}_{pc} \begin{bmatrix} \Gamma_1 \tilde{Z}_{cc} \\ j\Gamma_2 \end{bmatrix}^{-1} \begin{bmatrix} \Gamma_1 \tilde{Z}_{cp} \\ \tilde{0} \end{bmatrix}. \tag{2.46}$$

When the excitation port is defined as the first port of the overall Z_p matrix, then $Z_p(1,1)$ is the input impedance of the antenna.

Simplified expressions for the overall impedance matrix can be obtained when the segmentation of a γ structure is considered only in terms of two segments, namely α and β, as shown in Fig.2.5. The continuous interconnection between α and β segments is replaced by a discrete number of connected ports, named c-ports on α-segment and d-ports on β-segment. Ports p and q are the external (unconnected) ports of α and β segments, respectively. The Z-matrices for α, β and γ segments, namely Z_α, Z_β and Z_γ, respectively, can be partitioned into submatrices corresponding to the external (unconnected) and connected ports as follows:

$$Z_\alpha = \begin{bmatrix} \tilde{Z}_{pp\alpha} & \tilde{Z}_{pc} \\ \tilde{Z}_{cp} & \tilde{Z}_{cc} \end{bmatrix}, \quad Z_\beta = \begin{bmatrix} \tilde{Z}_{dd} & \tilde{Z}_{dq} \\ \tilde{Z}_{qd} & \tilde{Z}_{qq\beta} \end{bmatrix}, \quad Z_\gamma = \begin{bmatrix} \tilde{Z}_{pp\gamma} & \tilde{Z}_{pq} \\ \tilde{Z}_{qp} & \tilde{Z}_{qq\gamma} \end{bmatrix} \tag{2.47}$$

Z_γ can be computed using the segmentation method [4,5] and is given by

$$Z_\gamma = \begin{bmatrix} \tilde{Z}_{pp\alpha} - \tilde{Z}_{pc}\tilde{Z}'_{dp} & \tilde{Z}_{pc}\tilde{Z}'_{dq} \\ \tilde{Z}_{qd}\tilde{Z}'_{dp} & \tilde{Z}_{qq\beta} - \tilde{Z}_{qd}\tilde{Z}'_{dq} \end{bmatrix} \tag{2.48}$$

where

$$Z'_{dp} = \left(\tilde{Z}_{cc} + \tilde{Z}_{dd}\right)^{-1} \tilde{Z}_{cp} \tag{2.49}$$

$$Z'_{dq} = \left(\tilde{Z}_{cc} + \tilde{Z}_{dd}\right)^{-1} \tilde{Z}_{dq} \tag{2.50}$$

The impedance matrix obtained by (2.48) is the same as in (2.46).

The c-shaped slotted rectangular patch antenna shown in Fig.2.6 is analyzed by MNM using the segmentation method. This antenna geometry is proposed for the miniaturization of the antenna. By cutting a slot along one of its radiating edges, the length of the path that the surface currents flow on the patch is increased. Consequently, the antenna resonates at a lower frequency compared to the rectangular patch. The antenna dimensions, substrate parameters

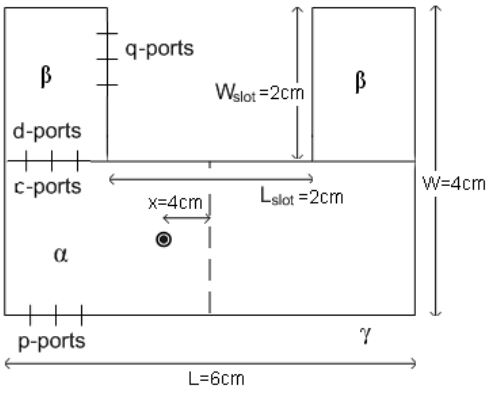

Figure 2.6: A c-shaped compact antenna obtained by segmentation of three rectangular segments, α and β to form the irregularly shaped γ segment. The substrate parameters are ϵ_r=2.33, thickness h=1.59mm, loss tangent=0.002

and the multiport model which is obtained by segmenting it into three RMSA's (one α and two β segments) are shown in Fig.2.6. The frequency analysis for the input reflection coefficient S_{11} is shown in Fig.2.7 where it is also compared to IE3D. Without the slot, c-shaped MSA becomes RMSA, and its resonance frequency is 1.606 GHz, with the slot, the resonant frequency is 1.142 GHz. The results show that the multiport analysis when used with the segmentation method gives good accuracy for this c-shaped antenna.

2.5 Desegmentation Method

The main distinction between the segmentation method and the desegmentation method is that the irregular shape (α circuit)is formed by subtracting a rectangular segment (β) from another rectangular segment (γ) in the desegmentation method. otherwise, the theory for the desegmentation method is similar to that of the segmentation method and same notations are used to denote the connected and external ports during the implementation of both methods.

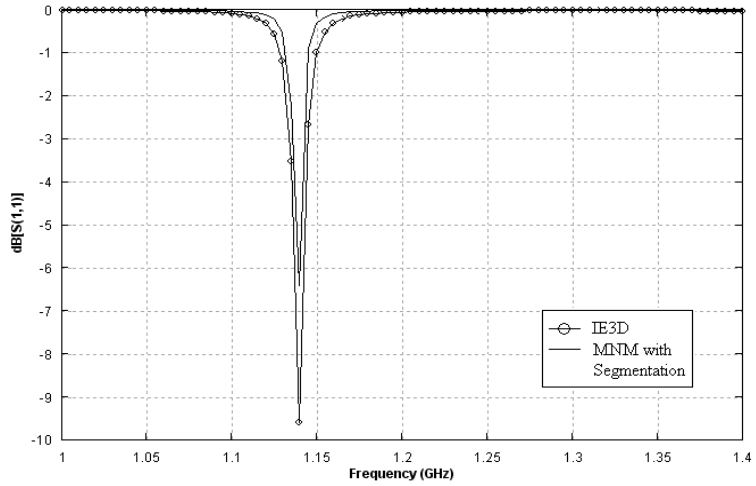

Figure 2.7: MNM frequency analysis of the c-shaped antenna for S_{11}dB using the segmentation method, and comparison to software program IE3D

The impedance matrix for the α circuit in terms of γ and β circuits is given by [7]

$$Z_\alpha = \begin{bmatrix} \tilde{Z}_{pp\gamma} - \tilde{Z}_{pq}\tilde{Z}'_{qp} & -\tilde{Z}_{pq}\tilde{Z}'_{qd} \\ -\tilde{Z}_{dq}\tilde{Z}'_{qp} & -\tilde{Z}_{dd\beta} - \tilde{Z}_{dq}\tilde{Z}'_{qd} \end{bmatrix} \tag{2.51}$$

with the submatrices given by

$$Z_\gamma = \begin{bmatrix} \tilde{Z}_{pp\gamma} & \tilde{Z}_{pq} \\ \tilde{Z}_{qp} & \tilde{Z}_{qq\gamma} \end{bmatrix}, \quad Z_\beta = \begin{bmatrix} \tilde{Z}_{dd} & \tilde{Z}_{dq} \\ \tilde{Z}_{qd} & \tilde{Z}_{qq\beta} \end{bmatrix}, \quad Z_\alpha = \begin{bmatrix} \tilde{Z}_{pp\alpha} & \tilde{Z}_{pc} \\ \tilde{Z}_{cp} & \tilde{Z}_{cc} \end{bmatrix} \tag{2.52}$$

where

$$\tilde{Z}'_{qp} = \left(\tilde{Z}_{qq\gamma} - \tilde{Z}_{qq\beta}\right)^{-1} \tilde{Z}_{qp} \tag{2.53}$$

$$\tilde{Z}'_{dq} = \left(\tilde{Z}_{qq\gamma} - \tilde{Z}_{qq\beta}\right)^{-1} \tilde{Z}_{dq} \tag{2.54}$$

The same c-shaped antenna that was studied in the segmentation analysis is used in the desegmentation analysis. The multiport model contains two rectangular patches (γ and β segments) that are desegmented to obtain the c-shaped patch (α segment) as shown in Fig.2.8. The results of the frequency analysis are shown in Fig.2.9. For comparison, they are plotted with the results of the segmentation method and IE3D. It can be seen that desegmentation method does not provide accuracy as good as the segmentation method.

For certain patch shapes particularly with slots, the easiest way to create the MNM is the desegmentation of a slot from the rectangular area. However, as observed in the previous simple

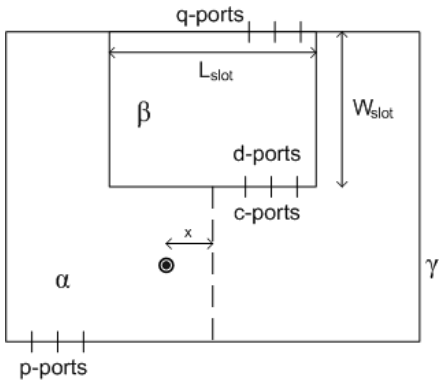

Figure 2.8: A c-shaped compact antenna obtained by desegmentation of two rectangular segments, γ and β to form the irregularly shaped α circuit. The substrate parameters are ϵ_r=2.33, thickness h=1.59mm, loss tangent=0.002

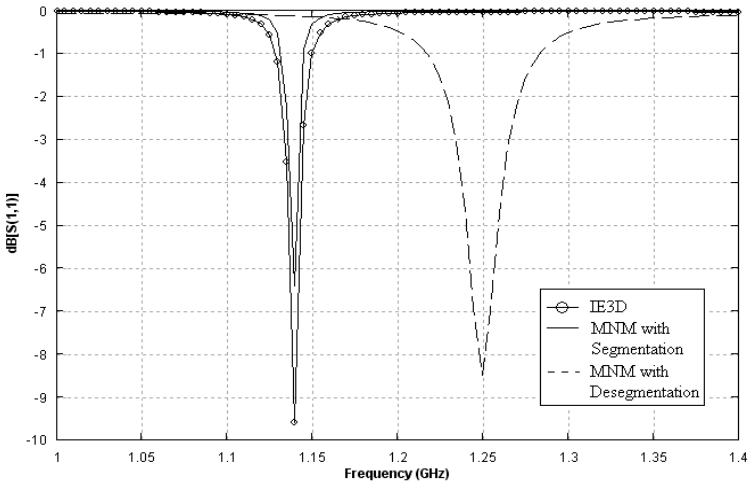

Figure 2.9: MNM frequency analysis of the c-shaped antenna for S_{11}dB using the desegmentation method, and comparison of the results with the results of the segmentation method and software program IE3D

example, this approach has accuracy problems. This accuracy problem becomes more severe as the dimensions of the slot that is subtracted from the rectangular patch becomes small compared to the patch. The sources of this error can be better understood by investigating the sub matrices in the overall impedance matrix in 2.51. The magnitudes of the entries of an impedance matrix corresponding to a segment are proportional to the size of the segment. Consequently, when there is a large ratio between the sizes of γ and β segments in the desegmentation method, there becomes a large difference between the magnitudes of the entries of the overall impedance matrix that that results in an ill-conditioned matrix equation. However, when the segmentation method is considered, general segments with similar sizes are combined to form the irregular shape and the problems associated with the condition number of the overall impedance matrix is not observed. A similar observation is also reported in [12], where it is stated that segmentation methods provides more accurate results compared to the desegmentation method, even though the segmentation methods requires the combination of more number of segments compared to a single subtraction in the desegmentation method.

To demonstrate the accuracy of the segmentation method with a more complex antenna structure, a stub loaded dual frequency antenna will be analyzed. This antenna can be realized by a pair of open circuited slots cut from one of the radiating edges of the rectangular patch as shown in Fig.2.10. The dual-frequency operation is obtained with slots resonant at one frequency and the rectangular patch resonant at an other frequency. The multiport model of the antenna is obtained by the segmentation of four rectangular segments. The antenna is analyzed by MNM with the dimensions and substrate parameter given in Fig.2.10. The results for the reflection coefficient are shown in Fig.2.11. Two operation frequencies are obtained at f_1=645 MHz and f_2=910 MHz that also confirmed by the results of IE3D. Another slotted patch example is the u-slot antenna that can be used to test the accuracy of the segmentation method in wide band applications. As shown in Fig.2.12, a rectangular patch with a u-shaped slot cut symmetrically around its center is called the u-slot antenna. With u-slot antenna it is possible to operate the antenna with bandwidths of 30-40%. The operation of the antenna is such that the resonant frequency of the rectangular patch and the slot are chosen to be close to each other so that wide band operation can be obtained. The patch dimensions and substrate parameters and given in Fig.2.12. The simulation results are shown in Fig.2.13 where 14% bandwidth is obtained. In all these slotted antennas examples, the MNM with segmentation method gives accurate results when compared to IE3D. With this conclusion, in all simula-

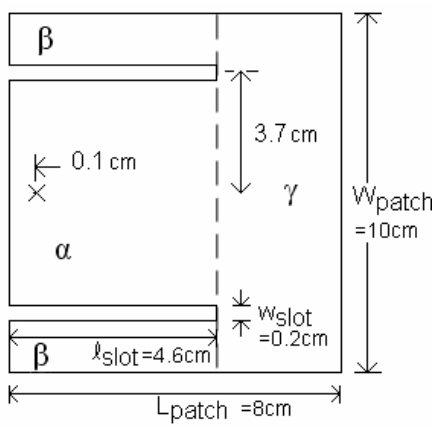

Figure 2.10: Dual frequency slot loaded antenna with substrate parameters ϵ_r=4.3, substrate thickness=1.59mm, loss tangent=0.02

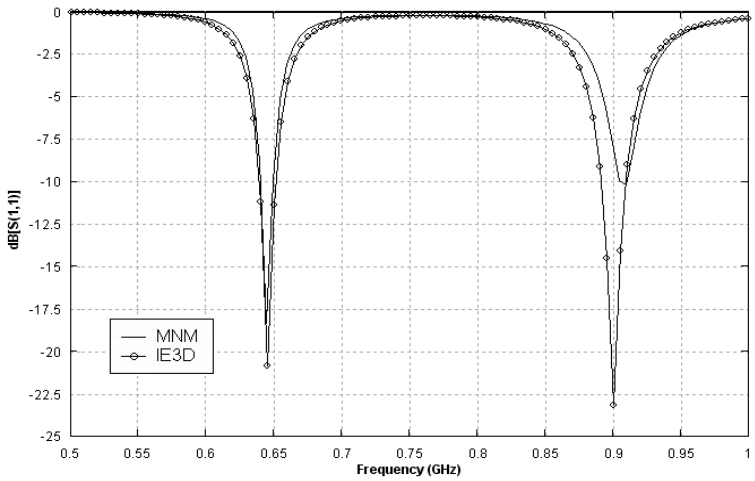

Figure 2.11: Frequency simulation of the dual frequency antenna for the reflection coefficient S_{11}, and the comparison of the results with IE3D

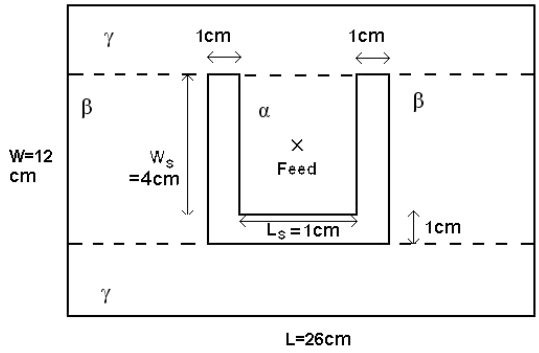

Figure 2.12: U-slot Antenna with substrate parameters ϵ_r=2.33, substrate thickness=2mm, loss tangent=0.02

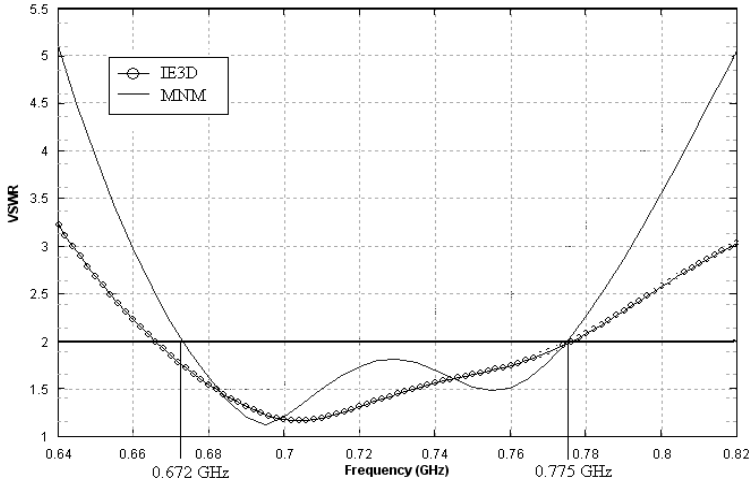

Figure 2.13: Frequency simulation of the u-slot antenna for VSWR, and the comparison of the results with IE3D

tions from this point on, the segmentation method will be used and the term MNM will refer to the multiport analysis using the segmentation method.

In the next chapter, vector Padé approximation will be presented. It is a mathematical approximation that is utilized in this thesis to develop a simple and an efficient design and analysis method by using the MNM.

CHAPTER 3

PADÉ AND VECTOR PADÉ APPROXIMATIONS

Let a function f be approximated in terms of a truncated power series. A Padé approximant of f is a rational function "matched" to this truncated power series whose degree is equal to the sum of the degrees of the numerator and the denominator of the rational function.

3.1 Padé Approximation

There are two approaches to the Padé approximation of a function. The first one is direct and easy to understand. The second approach is more complicated but also more comprehensive. The Padé approximation of a function $f(s)$, where s is the complex variable, is the ratio of two polynomials where the one in the numerator is of degree p and the one in the denominator is of degree q. The approximation is obtained by equating the Padé approximants f(s) to its power series expansion up to a degree (p+q) [28, 29], as shown in the following equation.

$$f(s) = \frac{a_0 + a_1 s + ... + a_p s^p}{b_0 + b_1 s + ... + b_q s^q} = M_0 + M_1 s + ... M_{p+q} s^{p+q} \tag{3.1}$$

where M_n's are the n^{th} moments of the power series. By matching two sides of (3.1) the coefficients in the numerator and denominator of the Padé approximation can be obtained from the following linear equation system.

$$\begin{bmatrix} M_p & M_{p-1} & \cdots & M_{p-q+1} \\ M_{p+1} & M_p & \cdots & M_{p-q+2} \\ \vdots & \vdots & \vdots & \vdots \\ M_{p+q-1} & M_{p+q} & \cdots & M_p \end{bmatrix} \begin{bmatrix} b_1 \\ b_2 \\ \vdots \\ b_q \end{bmatrix} = - \begin{bmatrix} M_{p+1} \\ M_{p+2} \\ \vdots \\ M_{p+q} \end{bmatrix} \tag{3.2}$$

and the numerator coefficients are obtained as:

$$a_r = \sum_{j=0}^{r} M_{r-j} b_j, \quad r = 0, 1, ..., p. \tag{3.3}$$

If the power series is expanded at s_0, then the moments in (3.2) and (3.3) have to be evaluated at $s = s_0$.

In the second approach to the Padé approximation, let f be a formal power series with complex coefficients

$$f(s) = c_0 + c_1 s + c_2 s^2 + c_3 s^3 + ... \tag{3.4}$$

where c_i's are the moments of the power series and s is the complex variable.

Let c be the linear functional on the space of complex polynomials defined by

$$c(x^i) = c_i \tag{3.5}$$

and

$$\begin{aligned} c((1 - xs)^{-1}) &= c(1 + xs + x^2 s^2 + ...) \\ &= c(1) + c(x)s + c(x^2)s^2 + ... \\ &= c_0 + c_1 s + c_2 s^2 + ... \\ &= f(s). \end{aligned} \tag{3.6}$$

Hence the problem of approximating f(s) is analogous to approximating

$$I = \int_a^b g(x) w(x) dx \tag{3.7}$$

where g(x) is replaced by an interpolation polynomial and this procedure is called "interpolatory quadrature" approximation [26]. In our case, in order to approximate the function f(s), the term 1/(1-xs) is replaced by its interpolation polynomial (Hermite) and then the functional c is applied which is analogous to integration. (3.6) can be re-written as

$$f(s) = c\left(\frac{1}{1 - xs}\right) \tag{3.8}$$

and the polynomial

$$R_k(x) = \frac{1}{1 - xs}\left(1 - \frac{v_k(x)}{v_k(s^{-1})}\right) \tag{3.9}$$

is the Hermite interpolation polynomial of degree k-1 of $(1 - xs)^{-1}$ where

$$v_k(x) = a_0 + ... + a_k x^k \tag{3.10}$$

is called the generating polynomial. The functional c is applied to R_k in order to obtain the approximation of f(s), the following results are obtained

$$c(R_k) = \frac{\tilde{w}_k(s)}{\tilde{v}_k(s)} \tag{3.11}$$

is the Padé approximation of f, where

$$w_k(s) = c\left(\frac{v_k(s) - v_k(x)}{s - x}\right) \tag{3.12}$$

and

$$\tilde{w}_k(s) = s^{k-1} w_k(s^{-1}) \tag{3.13}$$

$$\tilde{v}_k(s) = s^k v_k(s^{-1}) \tag{3.14}$$

(3.13) and (3.14) shows that $c(R_k(x))$ is a rational function whose numerator has a degree at most k-1 and whose denominator has a degree at most k. Such rational functions are called Padé approximants of f(s), and they are denoted by f[k-1/k](s). Thus, the approximation of f(s) can be expressed as

$$\begin{aligned} c(R_k(x)) &= c\left(\frac{1}{1 - xs}\right) - \frac{s^k}{\tilde{v}_k(s)} c\left(\frac{v_k(x)}{1 - xs}\right) \\ &= f(s) + O(s^k) \end{aligned} \tag{3.15}$$

where the error term can be expanded as

$$\begin{aligned} &c(R_k(x)) = f(s) - \\ &\frac{s^k}{\tilde{v}_k(s)} c\left(v_k(x)\left(1 + xs + ... + x^{k-1}s^{k-1} + \frac{x^k s^k}{1 - xs}\right)\right) \end{aligned} \tag{3.16}$$

In order to obtain the unknown coefficients $a_0, ..., a_k$ of the approximation, the error term is equated to zero leading to k equations with k unknowns.

$$c(x^i v_k(x)) = 0 \quad for \quad i = 0, ..., k - 1. \tag{3.17}$$

When the solution of the coefficients are substituded in (3.11) it gives the same results as in (3.2) and (3.3).

3.2 Vector Padé Approximation

The term vector Padé approximation is used for vector valued rational functions with a common denominator approximating simultaneously several functions $f_1, ..., f_m$ [26]. The main ideas of scalar approximation are kept and extended to this case.

Let $\bar{F} = (f_1, ..., f_d)$. $\bar{F}$ is supposed to be expanded into a power series with coefficients in C^d.

$$\bar{F}(s) = \sum_{i \geq 0} \bar{\Gamma}_i s^i, \tag{3.18}$$
$$\bar{\Gamma}_i \in C^d, s \in C^d$$

For each $\alpha = 1, ..., d$

$$f_\alpha(s) = \sum_{i \geq 0} c_i^\alpha s^i, \tag{3.19}$$

$$\bar{\Gamma}_i = (c_i^1, ..., c_i^d)^T \tag{3.20}$$

The linear functional is defined as $\Gamma : \bar{\Gamma}(x^i) = \bar{\Gamma}_i$. Similar to scalar Padé approximation, the generating polynomial is given as

$$v(s) = a_0 + ... + a_k s^k \tag{3.21}$$

and

$$\bar{W}(s) = \bar{\Gamma}\left(\frac{v_k(s) - v_k(x)}{s - x}\right) \tag{3.22}$$

then

$$\bar{\Gamma}(P(s)) = \frac{\tilde{W}(s)}{\tilde{v}(s)} \tag{3.23}$$

is the Padé approximation of the vector of functions $\bar{F}$ with $P(s)$ being the Hermite polynomial. Each component of $(\tilde{W}(s)/\tilde{v}(s))_\alpha$ is the Padé approximation of f_α for $\alpha = 1, ..., d$.

The error in the approximation can be written as

$$\begin{aligned} \bar{F}(s) - \bar{\Gamma}(P(s)) &= \frac{s^k}{\tilde{v}(s)} \bar{\Gamma}\left(\frac{v(x)}{1 - xs}\right) \\ &= \frac{s^k}{\tilde{v}(s)} \sum_{i \geq 0} \bar{D}_i s^i \end{aligned} \tag{3.24}$$

where

$$\bar{D}_i = \bar{\Gamma}(x^i v(x)) \tag{3.25}$$

In order to obtain the unknown coefficients $a_0, ..., a_k$ the error term is equated to zero so $\bar{D}_i = 0$ represents d scalar equations with respect to the coefficients of v as unknowns.

The generating polynomial v for "vector Padé approximation" is denoted by P_r, and the vector Padé approximation is given as

$$F[r - 1/r] = \frac{\tilde{W}(s)}{\tilde{P}_r(s)} \tag{3.26}$$

where r is the order of the denominator in the approximation and is defined as $r = nd + k$, where d is the total number of functions to be approximated in vector $\bar{F}$. The constant n and k are integers determined such that $0 \leq k \leq d$, and they must satisfy $r = nd + k$ for [r-1/r] type approximation.

The expression for P_r is given as

$$P_r(s) = \frac{\begin{vmatrix} \Gamma_0 & \cdots & \Gamma_r \\ \vdots & \cdots & \vdots \\ \Gamma_{n-1} & \cdots & \Gamma_{n+r-1} \\ \Gamma_n^{(k)} & \cdots & \Gamma_{n+r}^{(k)} \\ 1 & \cdots & s^r \end{vmatrix}}{\begin{vmatrix} \Gamma_0 & \cdots & \Gamma_{r-1} \\ \vdots & \cdots & \vdots \\ \Gamma_{n-1} & \cdots & \Gamma_{n+r-2} \\ \Gamma_n^{(k)} & \cdots & \Gamma_{n+r-1}^{(k)} \end{vmatrix}} \tag{3.27}$$

where each row $(\Gamma_i \cdots \Gamma_{r+i}$ represents d scalar rows formed by the components. The last row $(\Gamma_n^{(k)} \cdots \Gamma_{n+r}^{(k)}$ represents the k first components of $(\Gamma_n \cdots \Gamma_{n+r})$.

To illustrate the computational aspects of vector Padé approximation, consider the approximant of type F[1/2] for the functions $f_1(t)$=cos(t) and $f_2(t)$=sin(t).

The functions and their Taylor series expansions up to 5^{th} order are given as

$$f_1(t) = 1 - (1/2)t^2 + (1/24)t^4... \tag{3.28}$$

and

$$f_2(t) = t - (1/6)t^3 + (1/120)t^5... \tag{3.29}$$

Following that

$$\Gamma_0 = \begin{bmatrix} 1 \\ 0 \end{bmatrix}, \quad \Gamma_1 = \begin{bmatrix} 0 \\ 1 \end{bmatrix}, \quad \Gamma_2 = \begin{bmatrix} -1/2 \\ 0 \end{bmatrix}, \quad \Gamma_3 = \begin{bmatrix} 0 \\ -1/6 \end{bmatrix}, ... \tag{3.30}$$

Consider $f[1/2](t)$ then k=2 and

$$v_2(t) = a_0 + a_1 t + a_2 t^2 \tag{3.31}$$

Thus,

$$\tilde{v}_2(t) = t^2 v_2(t) = a_2 + a_1 t + a_0 t^2 \tag{3.32}$$

and $W(t)$ can be obtained from

$$W(t) = \Gamma\left(\frac{v(x) - v(t)}{x - t}\right) \tag{3.33}$$

The numerator of $W(t)$ can be evaluated as

$$v(x) - v(t) = a_0 + a_1 x + a_2 x^2 - a_0 - a_1 t - a_2 t^2 \tag{3.34}$$

$$= a_1(x - t) + a_2(x - t)(x + t) \tag{3.35}$$

Then, the rational function becomes

$$\frac{v(x) - v(t)}{x - t} = a_1 + a_2(x + t) \tag{3.36}$$

and $W(t)$ is obtained as

$$W(t) = \Gamma(a_1) + \Gamma(a_2(x + t)) \tag{3.37}$$

$$= \Gamma_0 a_1 + \Gamma_0 a_2 t + \Gamma_1 a_2 \tag{3.38}$$

with $\Gamma_i' s$ being vectors.

Also,

$$\tilde{W}_1(t) = tW(t^{-1}) = \Gamma_0 a_2 + t(\Gamma_0 a_1 + \Gamma_1 a_2) \tag{3.39}$$

and the Padé approximation of vector $\bar{F}$ becomes

$$F[1/2](t) = \frac{\tilde{W}_1(t)}{\tilde{v}_2(t)} = \frac{\Gamma_0 a_2 + t(\Gamma_0 a_1 + \Gamma_1 a_2)}{a_2 + a_1 t + a_0 t^2} \tag{3.40}$$

To find the coefficients, we use orthogonality condition as

$$\Gamma(x^i v_2(x)) = 0 \tag{3.41}$$

Imposing the condition for i=0,1 gives

$$a_2 = 1$$

$$\Gamma(x^0 v_2(x)) = 0 \tag{3.42}$$

which results as

$$\Gamma(a_0 + a_1 x + a_2 x^2) = 0 \tag{3.43}$$

or

$$a_0\Gamma_0 + a_1\Gamma_1 + a_2\Gamma_2 = 0 \tag{3.44}$$

Similar equations as can be obtained for i=2 as

$$a_0\Gamma_1 + a_1\Gamma_2 + a_2\Gamma_3 = 0 \tag{3.45}$$

These last two equations can be solved for a_1, and a_0 yielding $a_0 = 1/2$, $a_1 = 0$ for f_1, and $a_0 = 1/6$, $a_1 = 0$ for f_2.

By substituting a_2=1, (3.39) becomes

$$\tilde{W}_1(t) = tW(t^{-1}) = \Gamma_0 + t(\Gamma_0 a_1 + \Gamma_1) \tag{3.46}$$

In order to find the vector Padé approximation, first we find the generating polynomial $P_2(t)$ by setting k=0 and n=1 such that for d=2 and r=2, r=nd+k is satisfied for $0 \leq k \leq d$.

$$P_2(t) = \frac{\begin{vmatrix} \Gamma_0 & \Gamma_1 & \Gamma_2 \\ 1 & t & t^2 \end{vmatrix}}{\begin{vmatrix} \Gamma_0 & \Gamma_1 \end{vmatrix}} \tag{3.47}$$

When evaluated for Γ_i values, the polynomial P_2 becomes

$$P_2(t) = t^2 + 1/2 \tag{3.48}$$

Therefore,

$$\tilde{P}_2(t) = t^2 P_2(t^{-1}) = 1 + (1/2)t^2 \tag{3.49}$$

Finally, the vector Padé approximation is

$$F[1/2] = \frac{\tilde{W}_1(t)}{\tilde{P}_2(t)} = \frac{\Gamma_0 a_2 + (\Gamma_0 a_1 + \Gamma_1 a_2)t}{1 + (1/2)t^2} \tag{3.50}$$

where $a_2 = 1$, $a_1 = 0$ for both functions as evaluated before. Substituting the corresponding sets from the moment vectors

$$F[1/2] = \frac{1}{1 + (1/2)t^2} \cdot \begin{bmatrix} 1 \\ t \end{bmatrix} \tag{3.51}$$

The graph with $0 < t < 12$ for the functions and their approximations are plotted in Fig.3.1 To show what a higher order approximation look like, vector Padé approximation F[3/4] is evaluated with the following vectors and polynomials:

The generating polynomial $v_4(t)$ is

$$v_4(t) = a_0 + a_1 t + a_2 t^2 + a_3 t^3 + a_4 t^4 \tag{3.52}$$

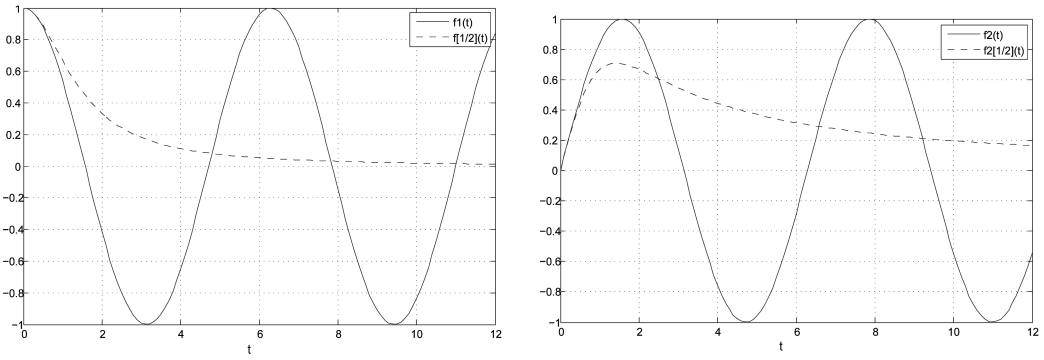

(a) (b)

Figure 3.1: Vector padé approximation F[1/2] for (a) f_1=cos(t) (b) f_2=sin(t)

and $\tilde{W}_3(t)$ is evaluated as

$$\tilde{W}_3(t) = \Gamma_0 a_4 + (\Gamma_0 a_3 + \Gamma_1 a_4)t + (\Gamma_0 a_2 + 2\Gamma_1 a_3 + \Gamma_2 a_4)t^2 + (\Gamma_0 a_1 + \Gamma_1 a_2 + \Gamma_2 a_3 \Gamma_3 a_4)t^3 \quad (3.53)$$

The constants are evaluated as for f_1 $a_0 = 0.005$, $a_1 = 0$, $a_2 = 0.0933$, $a_3 = 0$, $a_4 = 1$, and for f_2 $a_0 = 0.0019$, $a_1 = 0$, $a_2 = 0.0612$, $a_3 = 0$, $a_4 = 1$. The generating polynomial P_4 for the vector Padé approximation is

$$P_4(t) = \frac{\begin{vmatrix} \Gamma_0 & \Gamma_1 & \Gamma_2 & \Gamma_3 & \Gamma_4 \\ \Gamma_1 & \Gamma_2 & \Gamma_3 & \Gamma_4 & \Gamma_5 \\ 1 & t & t^2 & t^3 & t^4 \end{vmatrix}}{\begin{vmatrix} \Gamma_0 & \Gamma_1 & \Gamma_2 & \Gamma_3 \\ \Gamma_1 & \Gamma_2 & \Gamma_3 & \Gamma_4 \end{vmatrix}} = t^4 + (1/10)t^2 + (1/120) \quad (3.54)$$

The vector Padé approximation is

$$F[3/4] = \frac{\tilde{W}}{\tilde{P}_2(t)} = \frac{\Gamma_0 + \Gamma_1 t + (\Gamma_0 0.0933 + \Gamma_2)t^2 + (\Gamma_1 0.0933 + \Gamma_3)t^3}{1 + (1/10)t^2 + (1/120)t^4} \quad (3.55)$$

The graph with $0 < t < 12$ for the functions and their approximations are plotted in Fig.3.2

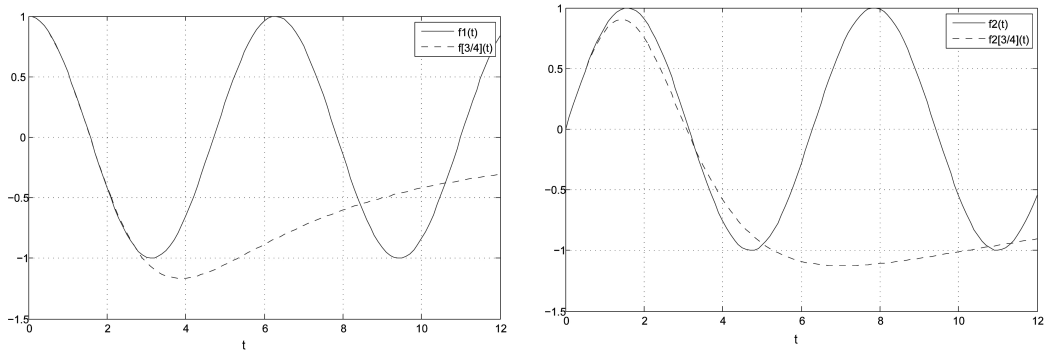

(a) (b)

Figure 3.2: Vector padé approximation F[3/4] for (a) f_1=cos(t) (b) f_2=sin(t)

CHAPTER 4

THE USE OF VECTOR PADÉ APPROXIMATION IN THE MNM ANALYSIS OF IRREGULARLY SHAPED PATCH ANTENNAS

This chapter addresses the application of the vector Padé approximation to the impedance matrix of an irregularly shaped patch antenna, obtained through the use of MNM. As discussed in the previous chapter, polynomials in the Padé approximations are obtained by using the Taylor series coefficients (moments) of the approximated function at the expansion point. For this reason, it is required to obtain the partial derivatives of the impedance matrix with respect to the approximation parameter, analytically. For regularly shaped patches, the derivatives can be obtained from the closed-form expressions of the impedance matrix entries. However, for irregularly shaped patches, the overall impedance matrix expression is composed of several sub matrices due to the segmentation process. Thus, in the following section, the formulation to evaluate the partial derivatives of the impedance matrix obtained through the use of segmentation method will be presented.

4.1 Evaluation of Derivatives for the Impedance Matrix

Consider the impedance matrix of the patch antenna obtained by the standard MNM given as

$$\tilde{Z} = \begin{bmatrix} Z_{11} & Z_{12} & \dots & Z_{1n} \\ \dots & & & \\ Z_{n1} & Z_{n2} & \dots & Z_{nn} \end{bmatrix} \tag{4.1}$$

where n is the total number of ports in the multiport model.

The vector Padé approximation of this impedance matrix will be in the form

$$\tilde{Z} \cong \bar{F}[q-1/q] \cong \frac{1}{(s-s_{p1})(s-s_{p2})...(s-s_{pq})} \begin{bmatrix} N_{11} & N_{12} & ... & N_{1n} \\ ... & & & \\ N_{n1} & N_{n2} & ... & N_{nn} \end{bmatrix} \tag{4.2}$$

where q is the degree of the denominator polynomial. N's are the numerator polynomials of the approximation of degree q-1. It should be noted that when the vector Padé approximation is obtained around the expansion point $s_0 (s_0 \neq 0)$, the variable s in (4.2) should be replaced by $(s - s_0)$.

In the evaluation of (4.2), a vector function is obtained by cascading the columns of the matrix in (4.1), then their derivatives are evaluated up to degree (2q-1). Evaluation of derivatives for regularly shaped patch is easy, because the analytic expression of the impedance function is known and can be differentiated with respect to any desired parameter. In order to evaluate the moments for the Z matrix of a irregularly shaped patch antenna, recall that overall Z matrix can be written in terms of sub matrices through the use of segmentation method as

$$\begin{bmatrix} \bar{V}_p \\ \bar{V}_c \end{bmatrix} = \begin{bmatrix} \tilde{Z}_{pp} & \tilde{Z}_{pc} \\ \tilde{Z}_{cp} & \tilde{Z}_{cc} \end{bmatrix} \begin{bmatrix} \bar{I}_p \\ \bar{I}_c \end{bmatrix} \tag{4.3}$$

where V_p, I_p and V_c, I_c are the voltages and currents at the p external and c internal connected ports.

From the segmentation analysis we get the overall network impedance matrix as

$$\tilde{Z}_p = \tilde{Z}_{pp} - \tilde{Z}_{pc} \begin{bmatrix} \Gamma_1 \tilde{Z}_{cc} \\ j\Gamma_2 \end{bmatrix}^{-1} \begin{bmatrix} \Gamma_1 \tilde{Z}_{cp} \\ 0 \end{bmatrix} \tag{4.4}$$

where Γ_1 and Γ_2 are interconnectivity matrices. $\tilde{Z}_p$ is the overall matrix of the final structure.

The derivatives of $\tilde{Z}_p$ in (4.4) can be obtained from the derivatives of the sub matrices $\tilde{Z}_{pp}$, $\tilde{Z}_{pc}$, $\tilde{Z}_{cp}$ and $\tilde{Z}_{cc}$. Thus, the n^{th} derivative of the overall matrix $\tilde{Z}_p$ can be written as

$$\frac{d^n}{ds^n}(\tilde{Z}_p) = (\tilde{Z}_{pp})^{(n)} - \left(\tilde{Z}_{pc} \begin{bmatrix} \Gamma_1 \tilde{Z}_{cc} \\ j\Gamma_2 \end{bmatrix}^{-1} \begin{bmatrix} \Gamma_1 \tilde{Z}_{cp} \\ 0 \end{bmatrix} \right)^{(n)} \tag{4.5}$$

where $^{(n)}$ stands for the n^{th} partial derivative with respect to s. In (4.5), the n^{th} derivative of the 2^{nd} term can be written in the matrix form by the triple product rule as

$$\left(\tilde{Z}_{pc} \begin{bmatrix} \Gamma_1 \tilde{Z}_{cc} \\ j\Gamma_2 \end{bmatrix}^{-1} \begin{bmatrix} \Gamma_1 \tilde{Z}_{cp} \\ 0 \end{bmatrix} \right)^{(n)} = \sum_{k=0}^{n} \sum_{p=0}^{k} \binom{n}{k} \binom{k}{p} \left(\tilde{Z}_{pc}\right)^{(p)} \left(\begin{bmatrix} \Gamma_1 \tilde{Z}_{cc} \\ j\Gamma_2 \end{bmatrix}^{-1} \right)^{(k-p)} \left(\begin{bmatrix} \Gamma_1 \tilde{Z}_{cp} \\ 0 \end{bmatrix} \right)^{(n-k)} \tag{4.6}$$

where $\binom{n}{k}$ and $\binom{k}{p}$ are the binomial coefficients.

Furthermore, the derivative of the inverse matrix

$$\tilde{Z} = \begin{bmatrix} \Gamma_1 \tilde{Z}_{cc} \\ j\Gamma_2 \end{bmatrix}^{-1} \tag{4.7}$$

can be evaluated by the following matrix identity

$$\frac{d^n}{ds^n}(\tilde{Z}^{-1}) = -\tilde{Z}^{-1}\tilde{Z}^{(n)}\tilde{Z}^{-1} \tag{4.8}$$

When using (4.8) to obtain the derivatives of the inverse matrix, some instability of the results may occur during the computations due to roundoff errors. This is especially more pronounced with matrices with higher order derivatives where the condition number of the matrix increases rapidly. Scaling can be used to improve ill-conditioning to an extend (scaling refers to multiplying all the derivatives by a constant). There are several formulations in the literature for the evaluation of this scaling constant. Also, more stable algorithms exist such as PVL (Pade Via Lanczos) [33] that can be used with little numerical degredation.

4.2 Vector Padé Approximation with Respect to Frequency

In the following examples, the frequency analysis of some irregularly shaped patch antennas are presented by applying the method of vector Padé approximated MNM. Approximations are performed with respect to the complex variable $s = j\omega$ with ω being the radian frequency.

4.2.1 C-shaped Patch Antenna

For the c-shaped microstrip antenna given in chapter 2.4, the poles of the approximation are analyzed in the complex s-plane. For this purpose, the poles of the approximation are evaluated for three different orders of approximation (F[1/2], F[2/3], F[3/4]) and at three different expansion points (s_0's). Since the resonance frequency of the antenna is 1.14 GHz, the expansion frequencies ($s_0 = j2\pi f_0$) are selected at 1.1 GHz, 1.15 GHz, and 1.20 GHz. Among the multiple poles (number of poles are equal to the order of the denominator polynomial), only a single pole is selected and plotted in the results. This selection is made according to the algorithm called "LAPACK - Linear Algebra Package" employed in Matlab where the

poles are given in an order $s_1, s_2, s_3, ..., s_q$. In this order, always the last pole is observed to be converging to the resonance mode of the antenna, and therefore this pole is plotted in the graphs.

The results are shown in Fig.4.1 where the poles are observed to converge towards the actual pole location in a trace of line, indicated by dotted lines for each expansion frequency. When the expansion frequency is closer to the resonance frequency, the radius of convergence narrows down in the s-plane. Consequently, closer and better convergences for all approximation orders are obtained.

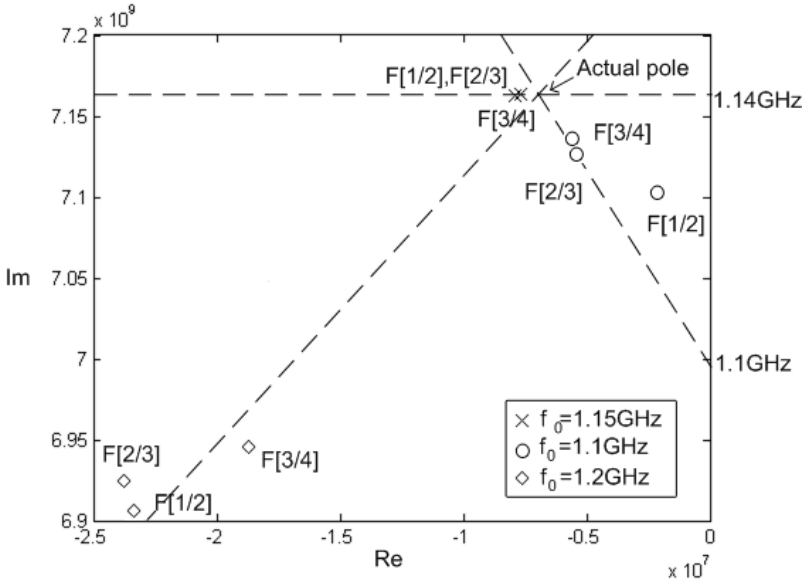

Figure 4.1: Poles of the approximation in the s-domain

In the second analysis, the frequency response of the antenna is obtained for the input reflection coefficient (s_{11}in dB) at different expansion frequencies. The approximation orders F[1/2] and F[2/3] are plotted in Fig.4.2(a) and Fig.4.2(b) for expansion frequencies f_0=1.1 and f_0=1.15 GHz, respectively. In obtaining these results, the antenna impedance matrix is vector Padé approximated, then the input impedance corresponding to feed port is used. The results of the simulation software IE3D are not plotted for the comparison with MNM since this was already done in chapter 2. From the graphs, it can be seen that higher order approximations and expansion frequencies closer to the resonance provide more accurate results.

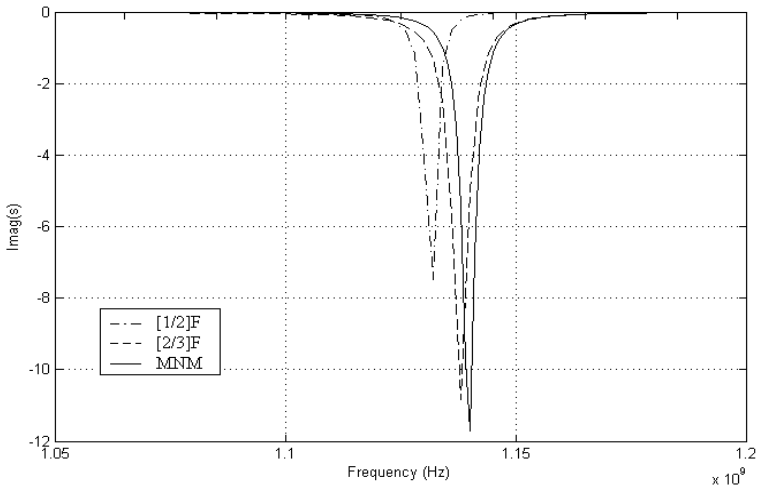

(a)

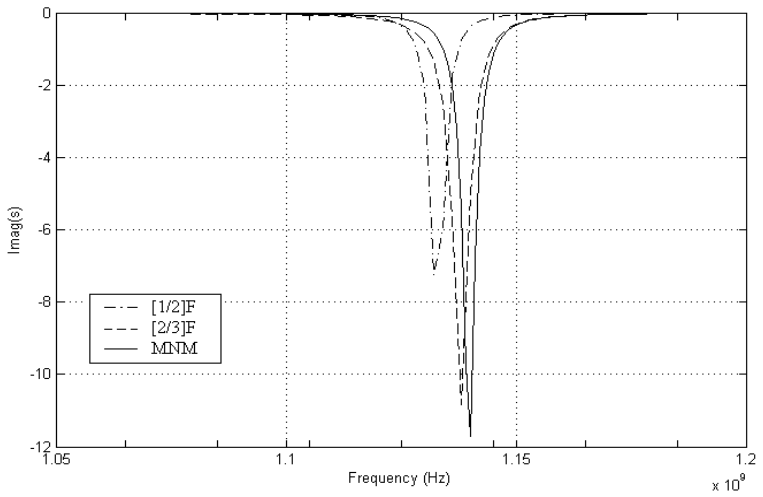

(b)

Figure 4.2: C-shaped antenna frequency analysis for s_{11}(dB) using approximation orders F[1/2] and F[2/3] at (a) f_0=1.1 GHz (b) f_0=1.15 GHz

In the last analysis, the effect of expansion frequencies on the accuracy of the results is presented. For this purpose, the vector Padé approximation is performed for various expansion frequencies between 1 and 1.35 GHz. Results are obtained where the x-axis denotes the expansion frequencies and the y-axis represents the imaginary part of the convergent pole corresponding to the Padé approximation at the associated expansion frequency. The graphs obtained for different orders of the approximation (F[1/2], F[2/3], and F[3/4]) are shown in Fig.4.3(a), (b) and (c), respectively. The resonance frequency of the antenna is shown by dotted line on the graphs. It is observed that the accuracy of the approximation improves as the poles of the approximation get closer to the resonance frequency of the antenna. Therefore it is possible to define a bandwidth of convergence that spans the expansion frequencies which provides accurate approximation. It is observed that higher order approximations yield broader bandwidth of convergence since they contain higher order derivatives in modeling the antenna characteristics.

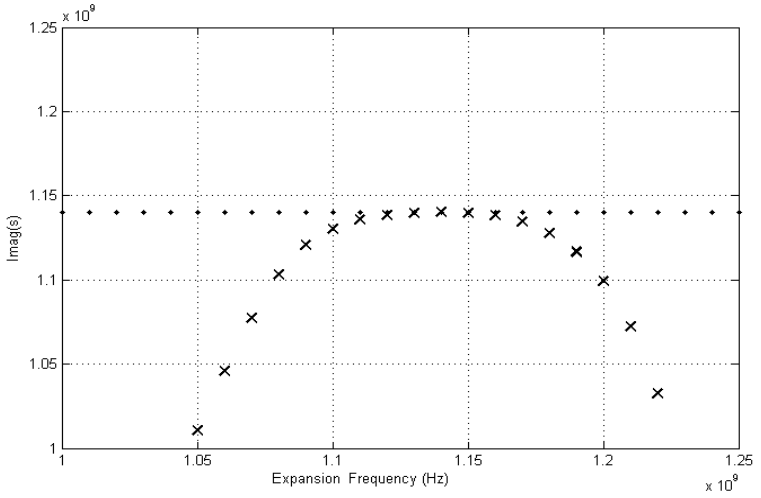

(a)

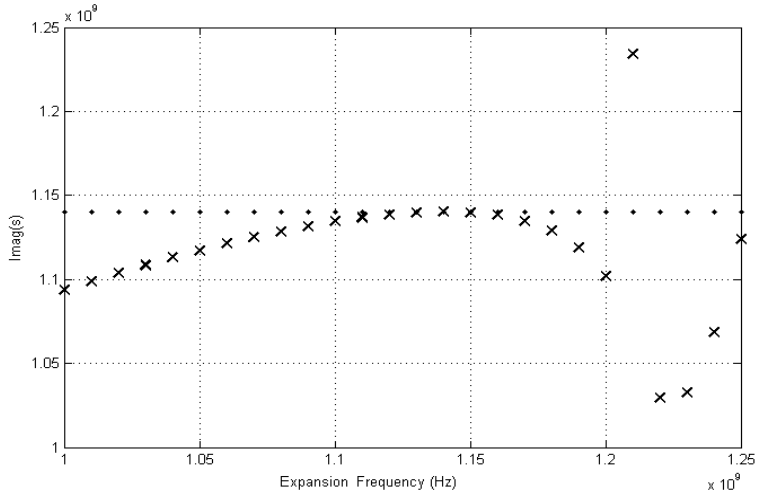

(b)

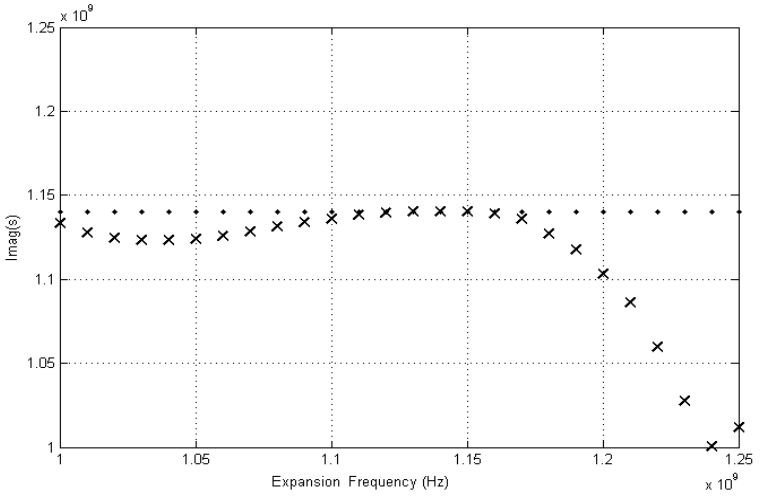

(c)

Figure 4.3: C-shaped antenna analysis: Pole locations with respect to expansion frequencies for the approximation orders (a) F[1/2], (b) F[2/3], (c) F[3/4].

4.2.2 Dual Frequency Antenna

The multiport network model of the slot loaded dual frequency rectangular microstrip patch antenna is shown in Fig.4.4.

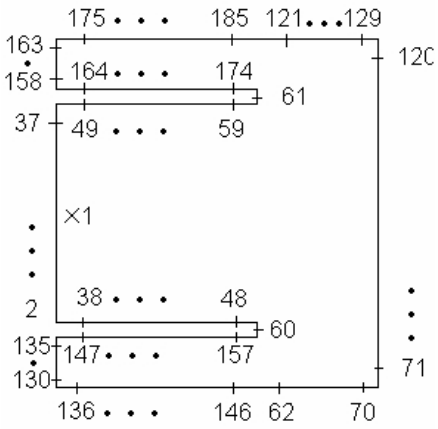

Figure 4.4: Multiport model of the dual frequency antenna

In the first analysis of this antenna, the vector Pade approximation is performed at various expansion frequencies between 0.5 - 1 GHz for approximation orders F[1/2], F[2/3], and F[3/4]. For each approximation order, q-1/q, the imaginary parts of q-1 poles are plotted with respect to the expansion frequencies in Fig.4.5(a), Fig.4.5(b) and Fig.4.5(c) for approximation orders F[1/2], F[2/3], and F[3/4], respectively. In the figures, dots indicate two resonant frequencies of the antenna (f=0.64 GHz, f=0.91 GHz). It can be observed from Fig.4.5(a) that with an approximation of order [1/2], only one of the resonances which is closer to the expansion frequency can be predicted. Moreover, for some expansion frequencies (7.6 - 8.4 GHz) between two resonance frequencies of the antenna, [1/2] order approximation fails to accurately model either of the resonances. But on the other hand, with an approximation of order [2/3], both of the resonances can be predicted with an acceptable accuracy for expansion frequencies between 7.8 - 8.2 GHz. Finally, with an approximation of order [3/4], both of the resonances can be modeled with an improved accuracy compared to order [2/3] for expansion frequencies between 7.8 - 8.6 GHz. Therefore it is concluded that the bandwidth of convergence becomes wider with increasing order of approximation.

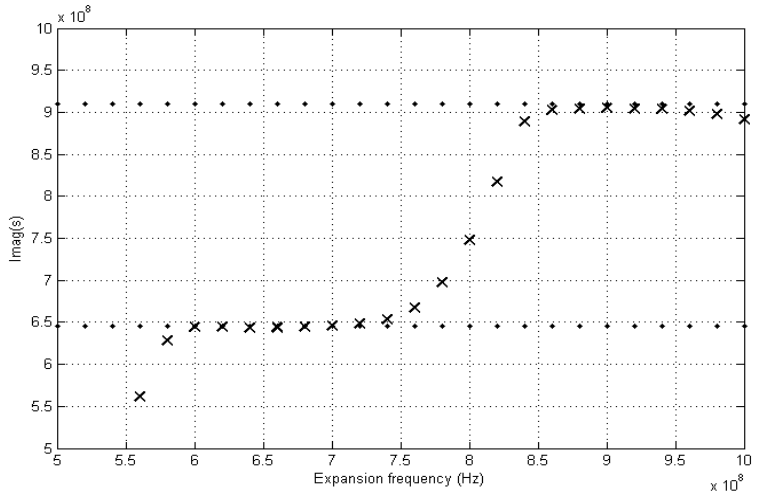

(a)

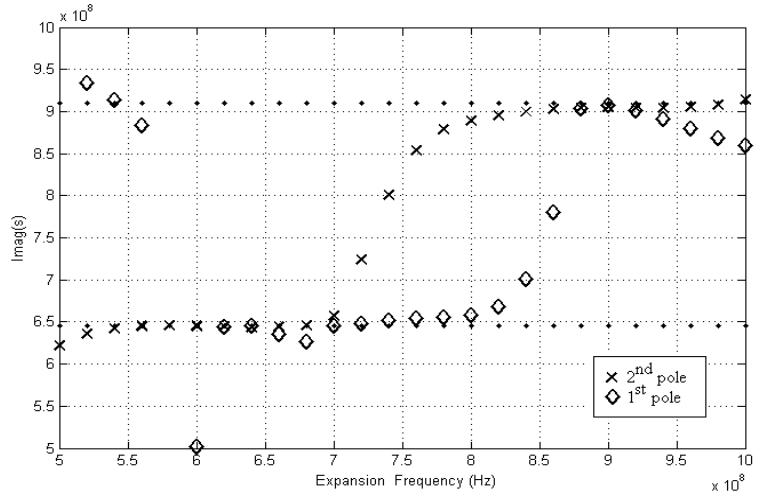

(b)

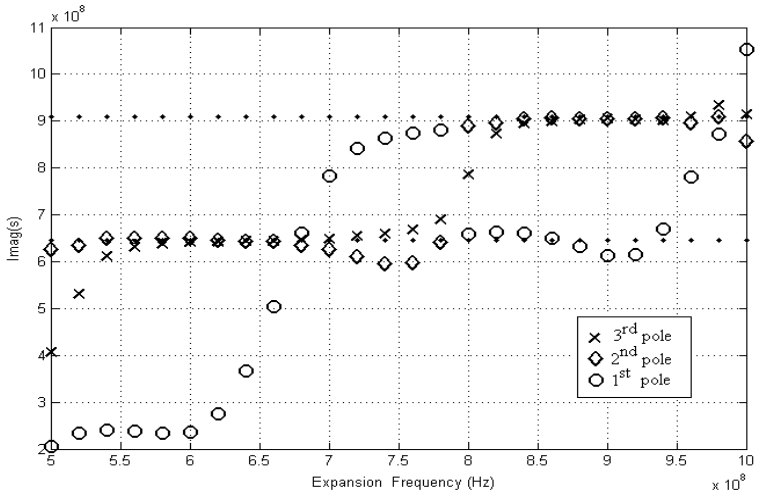

(c)

Figure 4.5: Dual frequency antenna analysis pole locations with respect to expansion frequencies for the approximation orders (a) F[1/2], (b) F[2/3], (c) F[3/4].

In the second analysis, the frequency response of the antenna is obtained at different expansion frequencies for approximation orders of F[1/2] and F[2/3]. The input return loss graphs at the expansion frequencies f_0=0.65 GHz, f_0=0.80 GHz and f_0=0.90 GHz are presented in Fig.4.5(a),(b) and (c) respectively. It is observed from the figures that if the frequency response of the antenna is required within such a large bandwidth (5-10 GHz), the accuracy of the approximation can not be considerably improved by increasing the order of approximation. Therefore, the approximation needs to be performed at more than one expansion point for the broadband analysis.

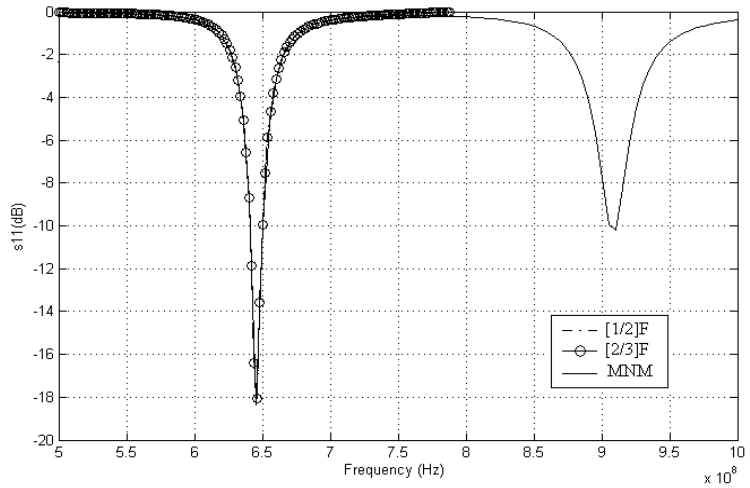

(a)

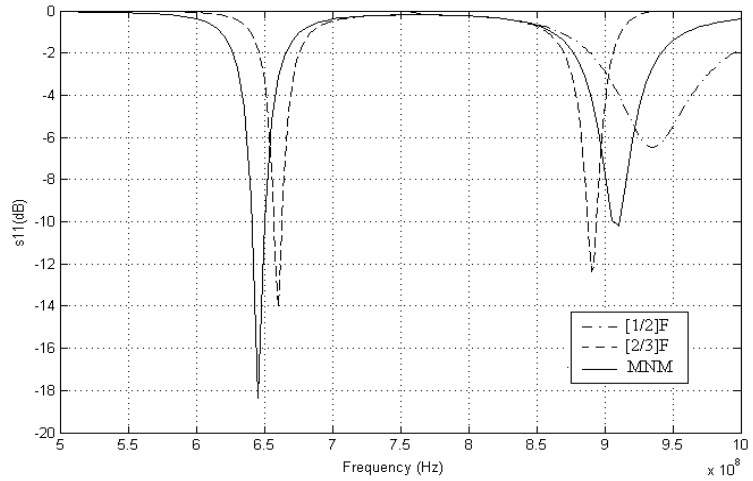

(b)

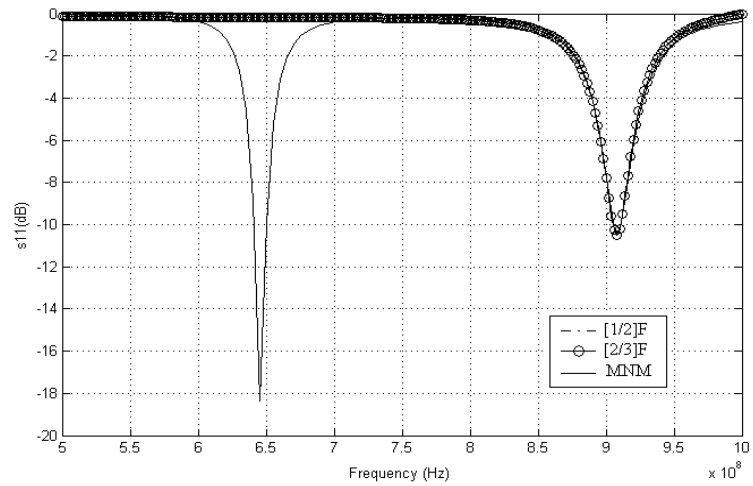

(c)

Figure 4.6: Dual frequency antenna frequency analysis for s11(dB) using approximation orders F[1/2] and F[2/3] at (a) f_0=0.65 GHz, (b) f_0=0.80 GHz, (c) f_0=0.90 GHz

4.2.3 U-slot Antenna

As the last example, the wideband microstrip patch antenna with a u-shaped slot is considered. The resonance frequency of the RMSA with u-slot is primarily determined by the length of the patch, and the total length of the u-slot. The lower resonance frequency is due to the resonance of the u-slot, and the higher resonance frequency is due to the excitation of the second-order mode of the patch. For the u-slot antenna introduced in chapter 2.4, the patch resonates at f=0.75 GHz with the dimensions W = 260 mm L=120mm, and the slot resonates at f=0.67 GHz with the dimensions L_s=60mm and W_s=60mm, yielding the antenna to operate with bandwidth of 14 % in the range 672-775 MHz for $vswr \leq 2$. The multiport model of the antenna is shown in Fig.4.7.

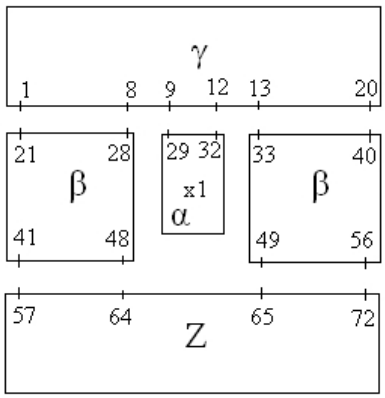

Figure 4.7: Multiport model of the U-slot antenna

Since the u-slot antenna resonates in a broad band of frequencies, poles of the approximation are scattered inside this bandwidth. Therefore, the pole analysis is not performed for this example and the results are presented only for the frequency response of the antenna at three different expansion frequencies. Fig.4.8 shows the frequency response for $s_{11}(dB)$ at expansion frequencies f_0=0.70 GHz, f_0=0.74 GHz, and f_0=0.78 GHz in parts (a),(b), and (c), respectively. The results are plotted for the approximation orders F[2/3], F[3/4], and compared to standard MNM where the closest match is obtained at f_0=0.74 GHz for the highest approximation order F[3/4].

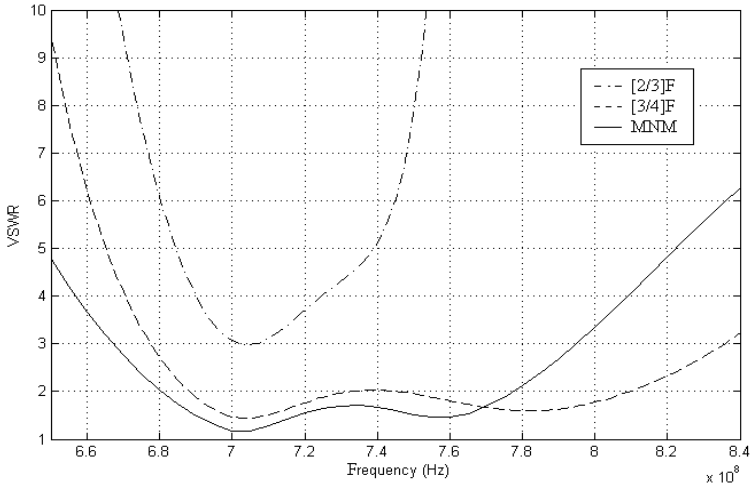

(a)

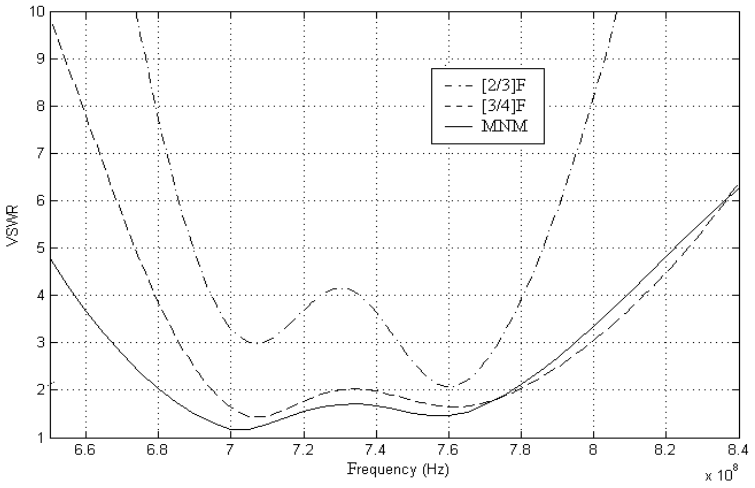

(b)

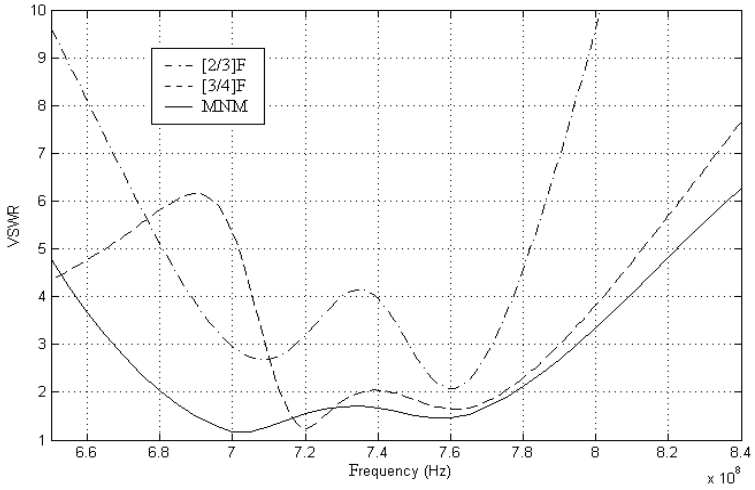

(c)

Figure 4.8: Frequency analysis of the u-slot antenna for VSWR at (a) f_0=0.70 GHz, (b) f_0=0.74 GHz, (c) f_0=0.78 GHz

In the summary of the frequency analysis for all the slotted antennas, the approximated method gives accurate results provided that the expansion frequency of the approximation is selected close to the actual resonant frequency. If the expansion frequency is away from the resonant frequency, then high order of approximations are necessary to get accurate results.

Following this section, computational efforts during the frequency analysis of the example antennas are presented for the standard MNM and the approximated method. The time efficiency of the proposed method over the standard MNM is also demonstrated through numerical examples.

4.2.4 Computational Efforts

When performing a frequency analysis by the standard MNM, the frequency band is divided into discrete frequency points. At each frequency point, first the Green's function, then the impedance matrices and the segmentation equations are evaluated. During these calculations, the most time consuming effort occurs in the calculation of the Green's function for multiports. Hence, for n-port antenna with m_f discrete frequency points, the total analysis time is roughly equal to

$$t_{MNM} \cong n t_s m_f \tag{4.9}$$

where t_s is the time required for the evaluation of the Green's function between any two-ports.

On the other hand, when the frequency response is obtained by performing vector Pade approximation, the number of evaluation steps is equal to the number of expansion frequencies used in the approximation. However for this case, not only the Green's function but also the moments have to be evaluated for multiports. Thus, for n-port antenna with m_e expansion points, the analysis time for the proposed method is roughly equal to

$$t_{Appr.MNM} \cong n(t_s + t_d) m_e \tag{4.10}$$

where t_d is the time required for the evaluation of the moments between two ports.

The relation between t_s and t_d can be written as

$$t_d \cong (0.6)(p + q) t_s \tag{4.11}$$

where (p+q) is the total number of moments that have to be evaluated in the approximation with p and q being the order of the numerator and denominator polynomials, respectively.

The factor (0.6) corresponds to the evaluation time for moments with respect to the evaluation time of the Green's function between two ports.

In the following sections, the computation times for the standard MNM and the MNM with vector Pade approximation will be compared for the example structures studied in the previous section.

4.2.4.1 Computational Efforts in the Analysis of the C-shaped Antenna

Computation times for the frequency analysis of the C-shaped frequency antenna between 1.0-1.25 GHz with the standard MNM and with the proposed method are presented in Table 4.1. In the proposed method, only one expansion point at f_0=1.15 GHz is considered. In the simulations, the Green's function is evaluated with 20 modes which is sufficient for good convergence. Both simulations are run on the same computer with dual-processor.

Table 4.1: Computational Efforts in Evaluating the Frequency Response of the C-shaped Antenna in the range 0.5-1 GHz for the Standard MNM and the Vector Padé Approximated MNM

Number of Evaluations	Procedure of the Standard MNM (in seconds)	Procedure of the Approx. MNM (in seconds) F[1/2],F[2/3],F[3/4]
50	6.76	-
100	11.4	-
1	-	0.23, 0.55, 0.81

The results in Table 4.1 show that the time advantage is very significant when using the proposed method. Also, the computation time and the number of evaluations increase proportionally in the standard MNM. Whereas in the proposed method, the computation time is more dependent on the approximation order than the number of evaluations.

It is possible to find the number of frequency steps necessary for the standard method to yield the same computation time as the proposed method. For this reason, the computation times given in (4.9) and (4.10) are equated as

$$nt_s m_f = n(t_s + t_d)m_e \tag{4.12}$$

Considering the approximation order F[2/3], the computation time for the evaluation of moments (t_d) can be written in terms of the computation time for the evaluation of the Green's function (t_s) by using (4.11) as

$$t_d \cong (0.6)(p+q)t_s = 3t_s \tag{4.13}$$

Substituting this result in (4.12) gives

$$m_f = 4m_e \tag{4.14}$$

Thus, approximately at 4 evaluation steps of the conventional method the two procedures yield the same time efforts which can be verified by the results in the Table 4.1. However, it is obvious from the resonance behavior of the antenna that 4 frequency points in the range 1-1.25 GHz is not sufficient to get accurate results.

4.2.4.2 Computational Efforts in the Analysis of the U-Slot Wideband MS Patch Antenna

Time efforts for obtaining the frequency response for the u-slot antenna are presented in Table 4.2. In the proposed method, there is a single evaluation made corresponding to the expansion frequency $f_0 = 0.72$ GHz. In the simulations 20 modes are used in the evaluation of the Green's function.

Table 4.2: Computational Efforts in Evaluating the Frequency Response of the U-slot Antenna in the range 0.65-0.84 GHz for the Standard MNM and the Vector Padé Approximated MNM

Number of Evaluations	Procedure of the Standard MNM (in seconds)	Procedure of the Approx. MNM (in seconds)F[2/3], F[3/4]
50	13.0	-
100	32.6	-
1	-	1.46, 2.35

The results in Table 4.2 are also in agreement with the previous formulations. The computation times are greater for the u-slot antenna than those for the c-shaped antenna because the number of ports used for the u-slot antenna is greater. There are 72 ports used in the u-slot antenna multiport model as shown in Fig.4.7.

4.2.4.3 Computational Efforts in the Analysis of the Dual Frequency Slotted Patch Antenna

The time efforts for obtaining the frequency response of the dual frequency antenna with standard MNM and the proposed method of the approximated MNM are presented in Table 4.3. In the proposed method there are 2 evaluations made corresponding to 2 expansion frequencies f_0 = 0.7 GHz and f_0 = 0.95 GHz. In the simulations of the dual frequency antennas, 40 modes are used in the evaluation of the Green's function.

Table 4.3: Computational Efforts in Evaluating the Frequency Response of the Dual Frequency Antenna in the range 0.5-1 GHz for the Standard MNM and the Vector Padé Approximated MNM

Number of Evaluations	Procedure of the Standard MNM (in seconds)	Procedure of the Approx. MNM (in seconds)F[2/3],F[3/4]
50	108	-
100	240	-
2	-	30,52

The time results in Table 4.3 are greater than the previous antenna examples. Again, this is due to larger number of ports used in the multiport model of the antenna.

In summary of these results, the new method of the Vector Padé approximated MNM offers significant computation time advantage in comparison to the conventional MNM. It should also be noted that the major disadvantage of the new procedure is that for the results to be accurate, the expansion frequency of the approximation must be selected in the vicinity of the actual resonant value.

In the last part of this chapter, the antenna dimensions are optimized for given resonant frequencies by the proposed method. To achieve this, the complex variable of the approximation (s=jω) is replaced by the length variable, (s=jL) or (s=jW). Subsequently, the derivatives are taken with respect to this length variable, and the approximation can be obtained. This time, the poles correspond to the dimensions where the antenna resonates.

4.3 Optimization of the Patch Dimensions by the Method of Vector Padé Approximated MNM

In order to design microstrip antenna patch dimensions, particularly the slot dimensions, by the method of vector Padé approximated MNM, the approximation needs to be performed with respect to the slot dimension to be optimized. Hence, the poles of the approximation will be the corresponding dimensions where the antenna resonates at the given frequency.

We know that for the approximation to be successful, the expansion value should be in the vicinity of the actual value of the resonance. Since there is no priori information for the optimum values of dimensions, the selection of the expansion value of the approximation is critical. First, an interval of uncertainty should be defined such that the optimum slot dimension is known to be somewhere inside this interval. Then, the convergent pole is traced with respect to the expansion values such that the evaluations stop when the difference between two successive poles are smaller than a pre-determined constant. At this point, the optimum dimension can be obtained from the convergent pole.

As an example, the c-shaped antenna shown in Fig.4.9 is optimized for its slot width W_s while keeping the slot length L_s constant. For this purpose, L_s is given two arbitrary values (2cm and 2.5cm), and W_s is aimed to be optimized at each of these L_s values by using the proposed method with approximation order F[2/3]. The resonant frequency is set constant at f=1.14 GHz, and the interval of search for W_s is selected to be [1,3]cm which is the feasible extension of the slot width in this geometry. Fig.4.10 shows the poles corresponding to different expansion points (W_s), where in part (a), the optimum slot width is obtained at 2cm and in part (b), the optimum slot width is obtained at 1.7cm corresponding to the slot lengths L_s=2cm and L_s=2.5cm, respectively. To confirm these results, the frequency response of the antenna with optimum slot dimensions are presented in Fig.4.11.

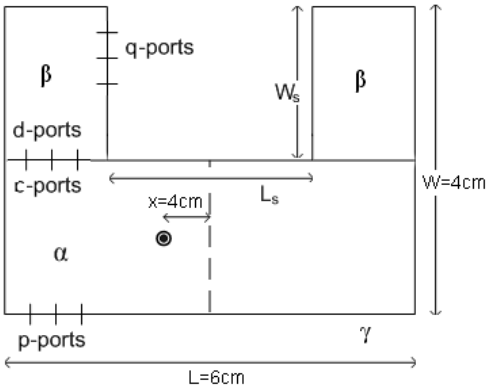

Figure 4.9: C-shaped antenna

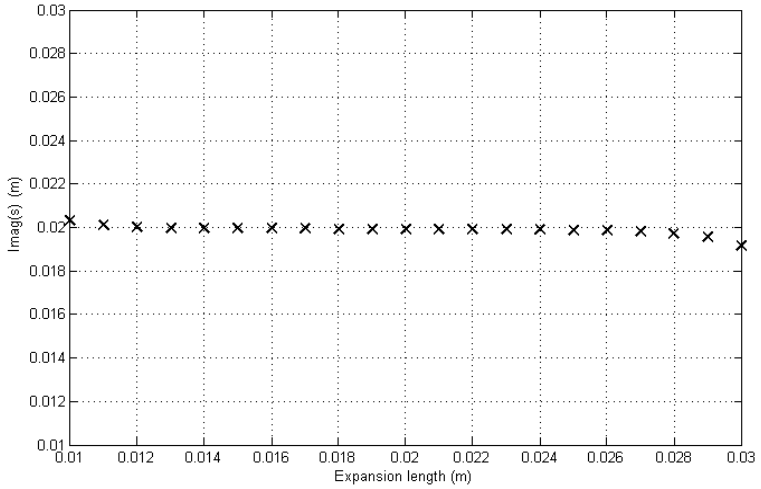

(a)

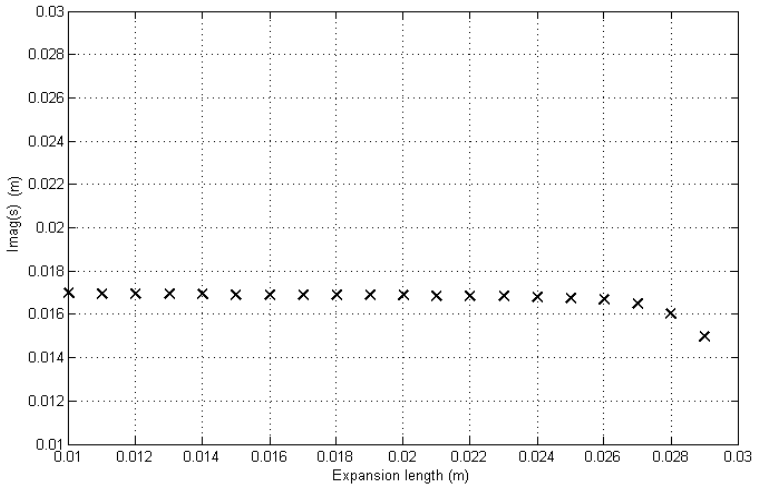

(b)

Figure 4.10: C-shaped antennas slot width optimization by using the approximation order F[2/3]. Pole dimensions for the slot width W_s versus the expansion values are plotted at slot lengths (a) L_s=2cm, (b) L_s=2.5cm.

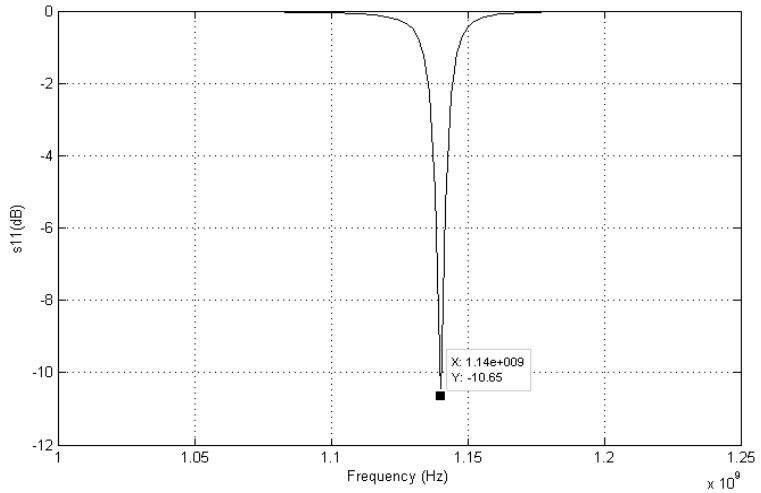

(a)

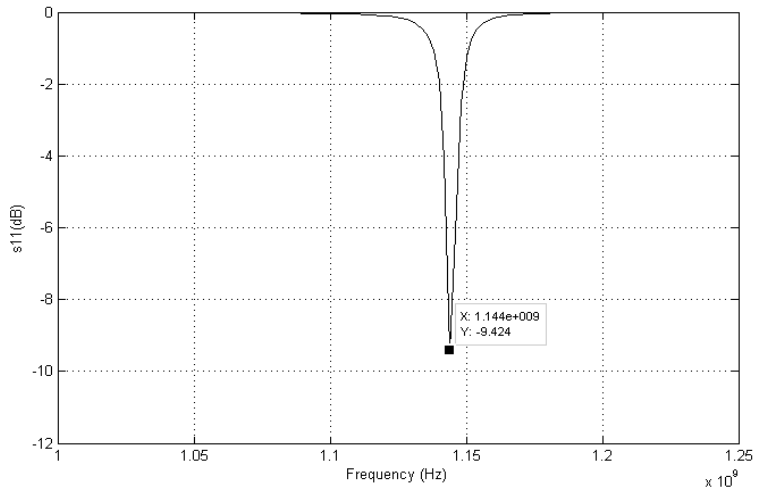

(b)

Figure 4.11: Frequency simulation of the c-shaped antenna by the MNM at the optimum slot dimensions (a) W_s=2cm,L_s=2cm, (b) W_s=1.7cm,L_s=2.5cm

In the next example, dual frequency antenna is optimized for its slot length L_s to operate the antenna at both 1.2 and 1.5 GHz. The antenna patch dimensions and the substrate parameters are shown in Fig.4.12.

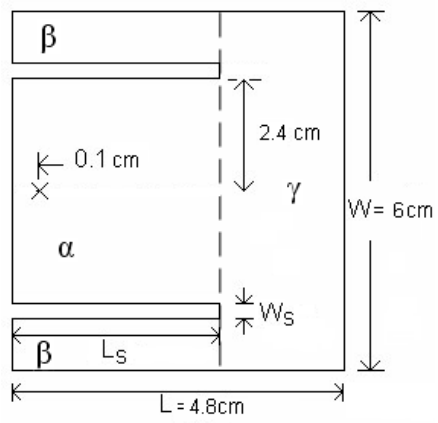

Figure 4.12: Dual frequency slot loaded antenna with substrate parameters ϵ_r=4.3, substrate thickness=1.59mm, loss tangent=0.02

The geometry of this slotted dual frequency antenna is proposed in [32] and it is reported that the upper resonant frequency of the antenna is mainly determined by the length of the rectangular patch. Therefore, first the length of the patch, L, is evaluated by using the cavity model as 4.8cm to yield the upper resonant frequency, 1.5GHz. Then, the patch width W is determined as 6cm by utilizing the same width-length ratio reported in [32]. On the other hand the length of the slot determines the lower resonant frequency, 1.2GHz. To optimize the length of the slot, L_s, first the width of the slot is chosen as W_s=0.2cm. Next, an appropriate interval is determined for the length of the slot which is chosen as [1,4]cm. Then, at 1.2 GHz the vector Pade approximation of order F[2/3] with respect to the slot length is obtained for different expansion points within this interval. The pole corresponding to this rational function approximation will yield the optimum length of the slot that the antenna resonates at 1.2 GHz. It is expected that the optimum length consequently the pole should be same for all expansion points. To verify this expectation, the pole corresponding to each expansion point is plotted in Fig.4.13. As it can be observed from the figure, only the poles that correspond to expansion points that are within the vicinity of the optimum length are same. The optimum slot length is observed to be L_s=2.6cm in the search interval of [1,4]cm. Fig.0.3 shows the frequency response of the antenna obtained by the multiport network model for this optimum value of the slot length. It can be observed that 1.2GHz resonance frequency is achieved by this length

but there is a slight shift in the upper resonance frequency. This is an expected result since the length of the patch was determined by an approximate formula. The higher resonance frequency can be tuned by adjusting the length of the antenna. To observe the effects of variations in the length of the slot on the frequency response of the antenna, MNM analysis are conducted for two different slot lengths, L_s=2 and 3.3cm, and the results are plotted in Fig.4.15 together with the results obtained for optimum slot length. As it is expected, the length of the slot determines the lower resonance frequency and it has a slight effect on the upper resonance frequency.

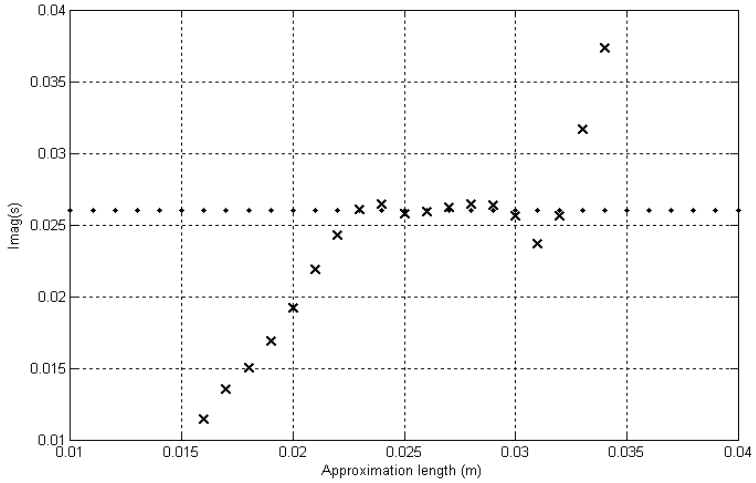

Figure 4.13: Pole dimensions for the slot length, L_s, versus the expansion values are plotted at slot width W_s=0.2cm for the approximation order F[2/3].

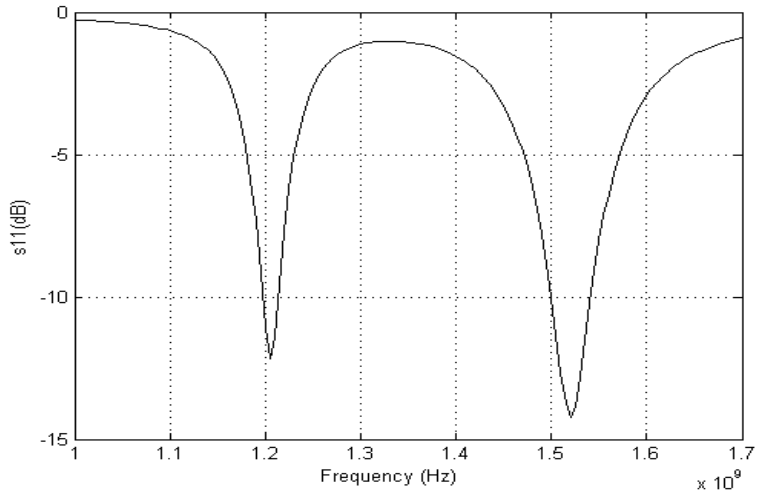

Figure 4.14: Frequency analysis of the dual frequency antenna by MNM at the optimum slot dimensions W_s=0.2cm, L_s=2.6cm.

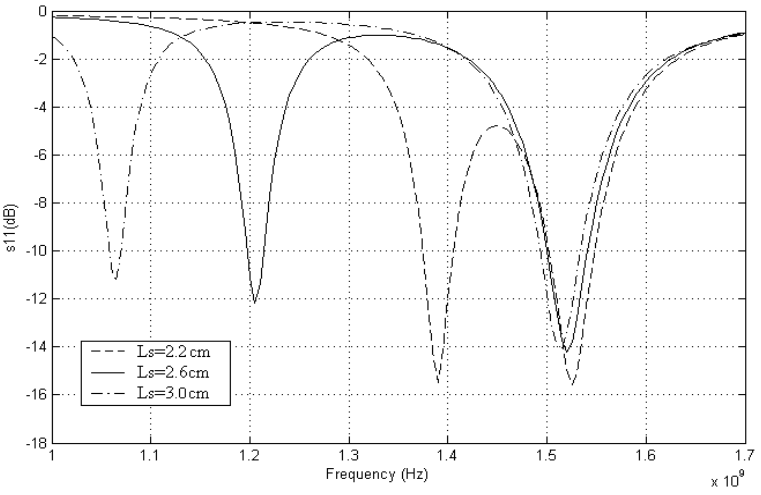

Figure 4.15: Frequency analysis of the dual frequency antenna by MNM at the slot dimensions W_s=0.2cm, L_s=2, 2.6 and 3.3cm.

Another slotted patch structure to obtain dual frequency operation can be realized by a rectangular microstrip antenna with two rectangular slots positioned close to the radiating edges. The antenna patch dimensions and the substrate parameters are shown in Fig.4.16.

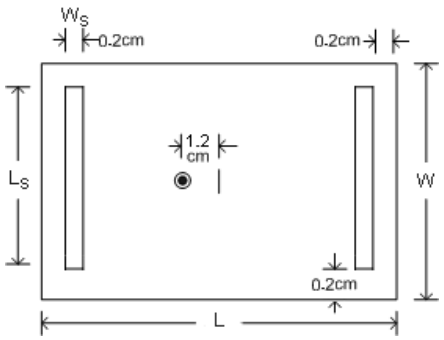

Figure 4.16: Dual frequency double slot antenna with substrate parameters ϵ_r=2.2, substrate thickness=1mm, loss tangent=0.02.

For this antenna configuration, the lower resonance frequency is mainly determined by the length of the patch. The patch length that yields the resonance at f_0=1.2 GHz is calculated to be L=8.2cm via cavity model. The upper resonance frequency of the antenna is determined by the length of the slot. Before optimizing the length of the slot, the width of the slot and the position of the slot need to be determined. Due to the operation principle of this dual frequency antenna, narrow width slots should be placed close to the radiating edges of the patch so that the fundamental mode is not disturbed. Therefore, the slot width W_s=0.2cm is selected and the slots are placed 0.2cm away from the radiating edges and the width of the patch is varied during the slot length optimization such that the slot is positioned 0.2cm away from the nonradiating edges as can be seen in Fig.4.16. In order to optimize one of the dimensions of the antenna, the utilization of the vector Padé approximation with respect to the optimized parameter is proposed in this thesis. However, it is observed in the previous example that the proposed method gives accurate results only if the expansion point is close to the optimum value. Therefore the expansion points for which the corresponding poles remain constant need to be determined to obtain accurate results. For this purpose, "Dichotomous search", which is a one dimensional search algorithm within a finite interval is adopted. First, the search interval defined as $[a_1, b_1]$ needs to be determined. For the current example, the search interval for the slot length can be selected according to the width of the patch. Next, the Pade approximation is performed with two expansion points: one at the midpoint of the interval $\frac{a_1+b_1}{2}$ and the other at the neighborhood of this point $\frac{a_1+b_1}{2}+\epsilon$. The poles of the ratio-

nal function approximation obtained via Pade method are compared. If the distance between the poles is less than a predetermined error criterion, the search algorithm stops, and the pole yields the optimum value. If the error criterion is not satisfied, then the search interval is divided into two and the same search algorithm is applied to each of these intervals. For the current example, the search interval for the length of the slot L_s is selected as [4,8]cm and the optimum slot length is obtained in the first iteration of the search algorithm since the mid-point of the search interval, 6cm, corresponds to an expansion point where the poles start to converge as can be seen in Fig.4.17. In this figure, the x-axis corresponds to the expansion points and the y-axis corresponds to the poles obtained from the Pade approximation at that expansion point. The optimum slot length is found to be L_s =6.4 cm. At the optimum slot dimensions, the results of the multiport network analysis are given in Fig.4.18. It can be observed from the figure that the lower resonance frequency which was determined by the length of the patch slightly shifts from the desired value due to approximate formula used in the calculation of the patch length. Moreover, the upper resonance frequency also slightly deviates from the expected value. This might be due to the assumption used in the proposed designed algorithm. It is assumed that the length of the slot is the sole parameter that determines the upper resonance frequency. However, it seems that the patch length has also a minor effect on the upper resonance frequency.

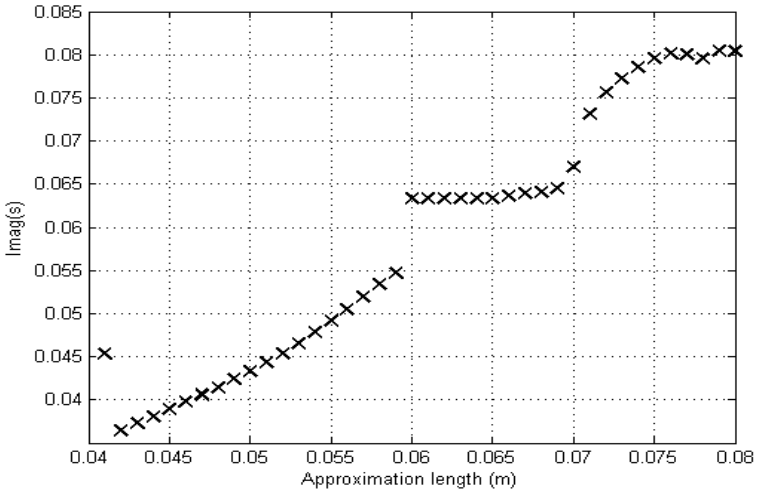

Figure 4.17: Poles of the approximation versus the expansion points for the approximation order F[2/3].

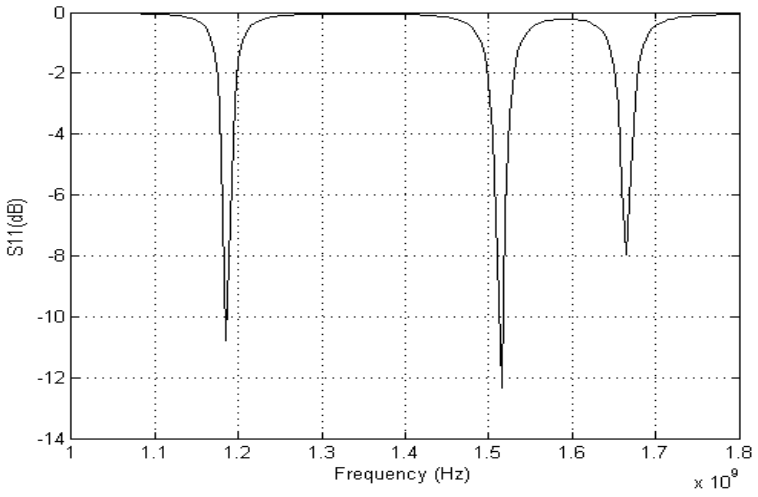

Figure 4.18: Frequency analysis of the dual frequency antenna by MNM at the optimum slot dimensions W_s=0.2cm, L_s=6.4cm.

CHAPTER 5

CONCLUSION

A new method for fast analysis and design of arbitrarily shaped microstrip antennas with slots has been developed. The proposed method combines multiport network model for microstrip antenna analysis with mathematical approximation called "vector Padé approximation".

The multiport network model is used in this thesis because it is simple and accurate analysis tool, and suitable for designing patch dimensions. Major limitation of this model is that it requires thin substrates. Although edge admittances can be used to account for the fringe fields, it's difficult to find an accurate model of edge admittances especially with increasing substrate thickness relative to wavelength. Also, multiport network model is not time efficient for wideband frequency analysis because the Green's function has to be evaluated for multiports in discrete frequency values. During these evaluations, the Green's function is analytically deducible only for regularly shaped patches such as rectangular, circular and triangular. For irregularly shaped patches such as slotted structures, the segmentation or desegmentation methods can be used to obtain the Green's function expression. In these methods, the overall patch shape is configured as the combination of regularly shaped segments (segmentation process) or the deduction of regularly shaped segments (desegmentation process).

Vector Padé approximation is used with the multiport network network model such that the impedance matrix corresponding to multiports is approximated by rational functions of polynomials with a common denominator. Then by using the poles of this approximation, frequency characteristics of the antenna can be obtained. To demonstrate the accuracy and efficiency of the proposed method, first the c-shaped antenna is analyzed in the frequency domain. It is observed that the proposed method gives accurate results when the expansion frequency of the approximation is selected near the actual resonant frequency. This band-

width of convergence is observed to be approximately 7% for the approximation order F[1/2] in the c-shaped antenna and improved for higher order approximations because more terms in the power series expansion are used in the approximation of the frequency characteristics. Second, the dual frequency antenna is analyzed in the frequency domain. The bandwidth of convergence for the expansion frequency is observed to be 15-20% using the approximation order F[1/2]. Since there are two resonant frequencies, two expansions frequencies can to be used to obtain the overall results. On the other hand, for high order approximations such as F[3/4], it is observed that poles converged to two resonant frequencies at a single expansion frequency within bandwidth of 6%. In the third example, u-slot antenna is analyzed and it is observed that approximation order at least F[3/4] was necessary to obtain accurate results when the expansion point is inside the resonance bandwidth.

In the frequency analysis, computations are faster with the new method because only the coefficients of the power series for the impedance matrix entries have to be evaluated. In the conventional method of multiport network analysis, the impedance matrix is evaluated for the entire discrete frequency domain. Computational efforts of frequency analysis are compared between the new method and the standard multiport network analysis. It is shown that the new method is approximately 10 times faster for the approximation order F[3/4] than the standard multiport analysis with 100 discrete evaluations in all antenna examples.

The proposed theory can be applied by using the approximation variable being antenna dimensions. Then, the method provides a single step computation for optimization of patch/slot dimensions instead of multiple evaluations in the frequency domain for different length combinations as done by the conventional algorithms. Examples for the optimization of the slot dimensions are carried out with the same antennas used in the analysis. The c-shaped antenna is optimized at two different resonant frequencies giving two sets of slot dimensions. Similarly, the dual frequency antenna is optimized for its slot dimensions at the 1.2 and 1.5 GHz GSM operation frequencies and the u-slot wideband antenna is optimized to operate between 672-775 MHz range. In these examples, one of the slot dimensions is optimized at a time. The optimum dimensions can be obtained by examining the pole locations against the expansion values. The optimum dimensions and therefore poles are positioned at the same value during the convergence bandwidth. In all simulations, the optimization results are verified by the multiport frequency analysis.

In the future work, the proposed method can be applied to other microstrip configurations such as gap coupled microstrip antennas by incorporating the mutual coupling networks in the multiport model or impedance matching networks by utilizing the design of transmission line dimensions.

REFERENCES

[1] T. Huynh, K.F. Lee, "Single-layer single-patch wideband microstrip antenna," *Electronics Letters*, Vol.31, No.16, pp. 1310-1312, Aug. 1995.

[2] S.K. Satpathy, V. Srinivasan, K.P. Ray, G. Kumar, "Compact Microstrip Antennas for Personal Mobile Communication," *Proceedings of IEEE Antennas and Propagation Soc. Int. Symp.*, pp. 245-248, 1998.

[3] B. Wang, Y.T. Lo, "Microstrip Antennas for Dual-Frequency Operation," *IEEE Transactions on Antennas and Propagation*, Vol.AP-32, No.9, pp. 938-943, Sept.1984.

[4] T. Okoshi and T. Miyoshi, "The planar circuit - An Approach to Microwave Integrated Circuitry," *IEEE Trans. Microwave Theory Tech.*, Vol. MTT-20, pp. 245-252. Apr. 1972.

[5] T. Okoshi, Planar Circuits for Microwave and Lightwaves. New York: Springer-Verlag, 1985.

[6] Chadha, K.C. Gupta "Segmentation Method Using Impedances Matrices for Analysis of Planar Microwave Circuits," *IEEE Transactions on Microwave Theory and Techniques*, Vol Mtt-29, No. 1, pp. 71-74, January 1981.

[7] P.C.Sharma, K. C. Gupta, "Desegmentation Method for Analysis of Two Dimensional Microwave Circuits," *IEEE Transactions on Microwave Theory and Techniques*, Vol Mtt-29, No. 10, pp. 1094-1098, October 1981.

[8] S.Ray, G. Kumar, "Compact Rectangular Ring Unequal Power Divider," *Proceedings of IEEE Microwave Theory and Tech. Soc. Int. Symp.*, pp. 1243-1246, 2003.

[9] M.Kishihara, K. Yamane, I. Ohta, T. Kawai, "A design of Multi-Stage, Multi-Way Microstrip Power Divider with Broadband Properties," *Proceedings of IEEE Microwave Theory and Tech. Soc. Int. Symp.*, pp. 69-72, 2004.

[10] C.Sharma, K.C. Gupta, "Analysis and Optimized Design of Single Feed Circularly Polarized Microstrip Antennas," *IEEE Transactions on Antennas and Propagation*, Vol.AP-31, pp. 949-955, No.6, Nov.1983.

[11] K.T.V. Reddy, "Multiport Network Model for Dual Feed Gap-Coupled Square Microstrip Antennas for Circular Polarization," *Proceedings of IEEE Antennas and Propagation Soc. Int. Symp.*, pp. 140-143, 2003.

[12] A.Holub, M.Polivka, "Application of MNM on Collinear Microstrip Patch Antennas," *Proceedings of IEEE Antennas and Propagation Soc. Int. Symp.*, Vol.1, pp. 61-64, 1997.

[13] G. Kumar, K.C. Gupta, "Directly Coupled Multiple Resonator Wide-Band Microstrip Antennas," *IEEE Transactions on Antennas and Propagation*, Vol.33, No.6, pp. 588-593, June 1985.

[14] F.Yang, X. Zhang, "A Broadband Dual Frequency Microstrip Antenna," *Proceedings of IEEE Antennas and Propagation Soc. Int. Symp.*, Vol.2, pp. 960-963, 1997.

[15] R. P. Parrikar, K.C. Gupta, "Multiport Network Model for CAD of Electromagnetically Coupled Microstrip Patch Antennas," *IEEE Transactions on Antennas and Propagation*, Vol.44, No.4, pp. 475-483, April 1998.

[16] A. Khajehnasiri, S. S. Naeini, "A generalized 2-D Multiport Model for Planar Circuits with Slots in Ground Plane," *IEEE Transactions on Antennas and Propagation*, Vol.55, No.5, pp. 1283-1292, May 2007.

[17] Y.Cailloce, M. Himdi, D.Thouroude, J.P.Daniel, "Analysis of Aperture Coupled Microstrip Antenna Using the Segmentation Method," *Electronics Letters*, Vol.32, No.12, pp. 1047-1048, June 1996.

[18] A. Benalla, K.C. Gupta, "Multiport Network Model and Transmission Characteristics of Two-Port Rectangular Microstrip Patch Antennas," *IEEE Transactions on Antennas and Propagation*, Vol.36, No.10, pp. 1337-1342, Oct. 1988.

[19] A. Benalla, K.C. Gupta, "Multiport Network Model for Rectangular Microstrip Patches Covered with a Dielectric Layer," *IEE Proceedings Pt.H.*, Vol.137, No.6, pp. 377-383, Dec. 1990.

[20] W.J.Krzysztofik, "Two Band Planar Array for GPS and/or GSM Terminals," *Proceedings of IEEE Antennas and Propagation Soc. Int. Symp.*, pp. 756-759, 2002.

[21] A. Benalla, K.C. Gupta, "Multiport Network Approach for Modeling the Mutual Coupling Effects in Microstrip Patch Antennas and Arrays," *IEEE Transactions on Antennas and Propagation*, Vol.37, No.2, pp. 148-152, Feb. 1989.

[22] G. Kumar, K.P. Ray, *B*roadband Microstrip Antennas, *Artech House*, 2003. pp. 391-392, 394.

[23] J.R. James, P.S. Hall, Handbook of Microstrip Antennas, *Peter Peregrinus*, 1989. pp. 488.

[24] M. Yuan, T. K. Sarkar, M. Salazar-Palma, "A Direct Discrete Complex Image Method From the Closed-Form Green's Functions in Multilayered Media," *IEEE Transactions on Antennas and Propagation*, Vol.54, No.3, pp. 1025-1032, March. 2006.

[25] J. M. Johnson, Y. Rahmat-Samii, "Genetic Algorithms and Method of Moments (GA/MOM) for the Design of Integrated Antennas," *IEEE Transactions on Antennas and Propagation*, Vol.47, No.10, pp. 1606-1614, Oct. 1999.

[26] P.G. Ciarlet, J.L. Lions, Handbook of Numerical Analysis, *North Holland*, 1994, Volume III.

[27] K. Gupta, R. Garg, R. Chadha, Computer-Aided Design of Microwave Circuits, *Artech House*, 1981. pp. 229-256.

[28] C. Brezinski, "Padé-Type Approximation and General Orthogonal Polynomials," *Intern. Ser. Number.* Math 50.

[29] C. Brezinski, "Outlines of Padé Approximation," *H.Werner et al. eds.*, Computational Aspects of Complex Anaylsis. Pp. 1-50.

[30] C.Brezinski, "Comparisons Between Vector and Matrix Padé Approximants," *Journal of Nonlinear Mathematical Physics.* June 21-26, 2002.

[31] D H. J. Pang, "Computer analysis of microwave planar circuit with impedance matrix," *Electron. Cm. (Japan)*. vol. 64-B. no. 9: pp.55-63. 1981.

[32] A.A. Deshmukh, K.P. Ray, "Stub loaded multi-band slotted rectangular microstrip antennas," *IET Microwaves, Antennas and Propagation*, Vol.3, pp. 529-535, 2009.

[33] Feng Ling, Dan Jian, Jian-Ming Jin, "Efficient Electromagnetic Modeling of Microstrip Structures in Multilayer Media," *IEEE Transactions on Microwave Theory and Techniques*, Vol 47, No 9, September 1999.

[34] Ramesh Garg, Prakash Bhartia, Inder Bahl, Apisak Ittipiboon, Microstrip Antenna Design Handbook, *Artech House*, 2000. pp. 258-260.

[35] ShiChai Chen, GuangCong Liu, XiangYu Chen, TingFen Lin, XiangGuo Liu, and ZhiQi Duan, "Compact Dual-Band GPS Microstrip Antenna Using Multilayer LTCC Substrate," *IEEE Antennas and Wireless Propagation Letters*. Vol.9, pp. 421-423. 2010.

APPENDIX A

Radiated Fields in MNM

The radiated fields in MNM are evaluated by the equivalent magnetic current densities along the radiating edges. The equivalent magnetic current density at the radiating edge is given by

$$M = \hat{n} \times \bar{E} \tag{A.1}$$

where $\hat{n}$ is the unit normal vector to the magnetic side wall for the radiating edge. By using the equivalent current approximation

$$K = -2(\hat{n} \times \bar{E}) \tag{A.2}$$

where the factor 2 comes from the image of the current source, the far field electric potential is given by [1]

$$F_x = \frac{\epsilon_0}{4\pi r} e^{-jk_0 r} \sum_{i=1}^{m} \int_{c_i} K_{ix}(r') e^{jk_0 r' cos\xi} dl(r') \tag{A.3}$$

$$F_y = \frac{\epsilon_0}{4\pi r} e^{-jk_0 r} \sum_{i=1}^{m} \int_{c_i} K_{iy}(r') e^{jk_0 r' cos\xi} dl(r') \tag{A.4}$$

where K_{ix} and K_{iy} are the components of magnetic current vectors along the x and y directions, and ξ is the angle between the two vectors. Since K has no component in the z-direction, F_z is zero.

Using the rectangular to polar transformation,

$$F_\theta = (F_x cos\phi cos\theta + F_y sin\phi cos\theta) \tag{A.5}$$

and

$$F_\phi = (-F_x sin\phi + F_y cos\phi) \tag{A.6}$$

E_θ and E_ϕ are obtained from F_θ and F_ϕ as

$$E_\theta = \eta H_\phi = jk_0 F_\phi \tag{A.7}$$

$$E_\phi = -\eta H_\theta = jk_0 F_\theta \tag{A.8}$$

The total radiated power P_r is obtained as

$$P_r = \frac{1}{120\pi} \int_0^{2\pi} \int_0^{\pi/2} (|E_\theta|^2 + |E_\phi|^2) r^2 sin\theta d\theta d\phi \tag{A.9}$$

Typical radiation patterns based on (A.7) and (A.8) are broadside with no sidelobes both in E-plane and H-plane. The radiation field approaches zero ar $\theta = \pi/2$. This is due to the image of the patch in the ground plane. The narrow patch in the direction of radiation (small W), broadens the H-plane pattern, while thinner substrate (small L) broadens the E-plane pattern.